# Geochemical characterization, U–Pb apatite geochronology, and geodynamic significance of olivine minette dykes from the Julian Alps, NE Italy

Francesco Narduzzi[1], Maurizio Ponton[1], Michele Marello[1], Marco Paulo de Castro[2], Gláucia Queiroga[2] and Angelo De Min[1]

[1]Department of Mathematics and Geosciences, University of Trieste, Via Weiss 8, 34128 Trieste, Italy and [2]Departamento de Geologia, Escola de Minas, Universidade Federal de Ouro Preto, Campus Morro do Cruzeiro, 35400-000 Ouro Preto, Minas Gerais, Brazil

**Abstract**

We investigated olivine minette dykes from the Rio Colan Valley of the Julian Alps (NE Italy) to provide new constraints on the mantle geochemistry underneath this extreme sector of the Italian Southern Alps. Petrographic observations, high Mg#s, high Cr and Ni contents, low $Dy/Yb_{CN}$ ratios and flat heavy rare earth element (REE) profiles imply these are primary magmas derived from a depleted peridotite with olivine and garnet as possible residual phases. However, high $K_2O$ and incompatible trace element contents, coupled with superchondritic Nb/Ta ratios, suggest that the source was modified into a rutile–phlogopite-bearing carbonated peridotite by multiple metasomatic events such as recycling of crustal material and carbonatitic metasomatism related to an old orogenic event and rutile-rich metasomatism linked to the Pangaea break-up. Laser ablation – multi-collector – inductively coupled plasma – mass spectrometer (LA-MC-ICP-MS) U–Pb geochronology of apatites from two dykes yielded differences between unforced and forced discordia ages up to ~45 Ma, likely due to the initial $^{207}Pb/^{206}Pb$ correction adopted. Nonetheless, because forced discordia and $^{206}Pb/^{238}U$ weighted mean ages are overall similar within the uncertainty, our preferred interpretation is that olivine minettes intruded and crystallized at ~67 Ma. The age and anorogenic signature of these magmas are consistent with the regional extensional tectonics in the Julian Alps due to the advance of the external Dinaric front following Adria plate eastward subduction. Eventually, we show also that Rio Colan magmas are geochemically hybrid products between lamprophyres and lamproites compared with similar Italian and Western Mediterranean volcanics.

**Author for correspondence:**
Francesco Narduzzi,
Email: narduzzi13@gmail.com

## 1. Introduction

Lamprophyres, lamproites and other mafic–ultramafic alkaline rocks (e.g. kimberlites and orangeites) record information on the depletion and metasomatic processes occurring as deep as the asthenospheric Earth's mantle and are genetically linked to major events of supercontinent break-up and amalgamation (Krmíček & Chalapathi Rao, 2022). Lamprophyres (see Le Maitre *et al.* 2002; Krmíček & Chalapathi Rao, 2022 for a review) are mesocratic and less commonly holomelanocractic, porphyritic rocks that usually occur as dykes and sills. They are characterized by phenocrysts of euhedral to subhedral mafic anhydrous (commonly hydrothermalized clinopyroxene ± olivine) and hydrous mafic (mica and/or amphiboles) minerals. These phenocrysts are immersed in a groundmass formed by the same mafic minerals in addition to occasional feldspars and/or feldspathoids. Lamprophyres are generally subdivided into three sub-groups, calc-alkaline, alkaline and ultramafic, with a further subdivision based on the proportion of light-coloured and mafic minerals. These rocks usually contain high amounts of $K_2O$ and/or $Na_2O$, $H_2O$, $CO_2$, S, $P_2O_5$ and Ba. On the other hand, lamproites contain $TiO_2$–$Al_2O_3$-poor phenocrystic phlogopite, groundmass poikilitic tetraferriphlogopite, $TiO_2$–$K_2O$ richterite, forsteritic olivine, $Al_2O_3$–$Na_2O$-poor diopside, non-stoichiometric Fe-rich leucite and Fe-rich sanidine (chemical ranges in Le Maitre *et al.* 2002; see also Lustrino *et al.* 2016 and Krmíček & Chalapathi Rao, 2022). All these minerals are not required, but the presence of primary plagioclase, melilite, monticellite, kalsilite, nepheline and Na-rich alkali feldspar, among many others, precludes a rock from being a lamproite. Like lamprophyres, lamproite nomenclature is based on the occurrence of primary minerals. Additionally, lamproites are ultrapotassic (molar $K_2O/Na_2O > 3$), perpotassic (molar $K_2O/Al_2O_3 > 1$), and peralkaline (molar $K_2O + Na_2O/Al_2O_3 > 1$) with Mg# ($Mg/(Mg + Fe^{2+}) > 70$, $FeO_{Tot}$ and $CaO < 10$ wt %, $Ba > 2000$ μg/g (commonly > 5000 μg/g), $TiO_2$ from 1 to 7 wt %, $Zr > 500$ μg/g, $Sr > 2000$ μg/g, $Zr > 500$ μg/g and $La > 200$ μg/g (Foley *et al.* 1987; Le Maitre *et al.* 2002).

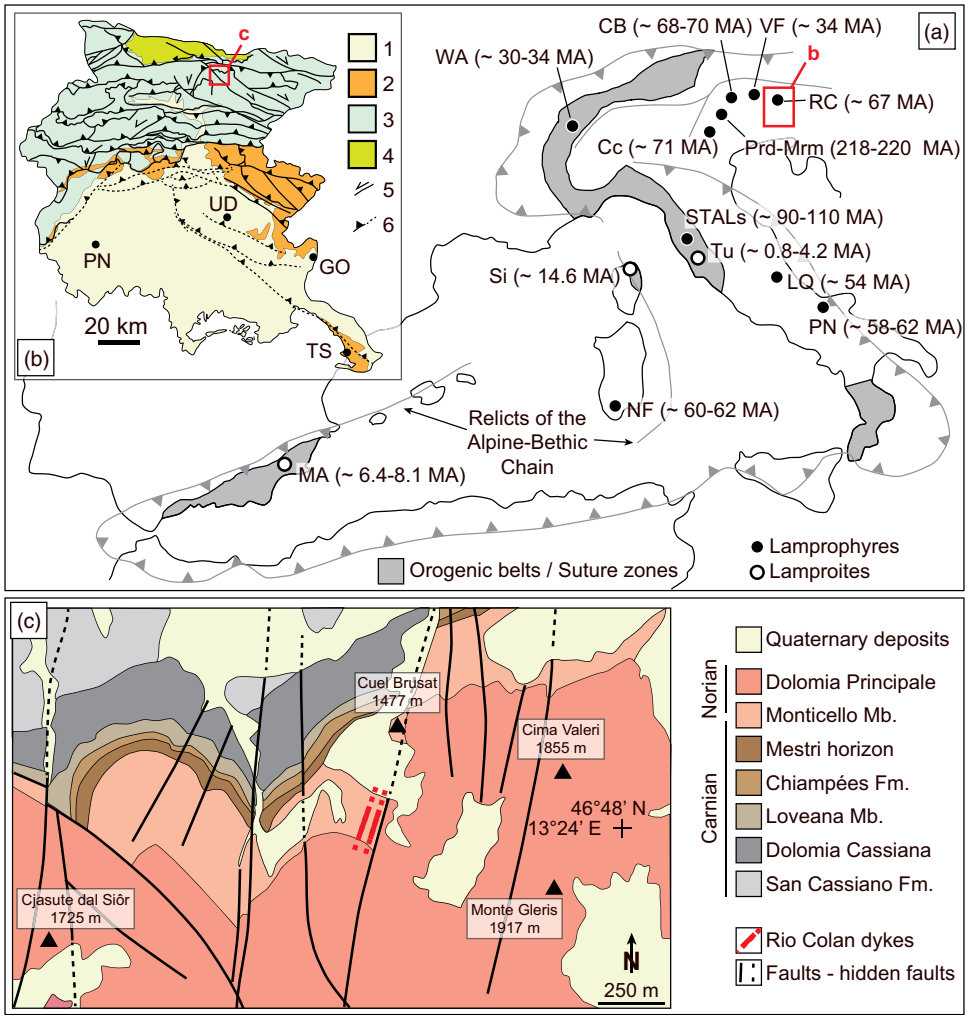


**Fig. 1.** (Colour online) (a) Lamprophyre and lamproite occurrences in the present-day Western Mediterranean area (modified from Prelević *et al.* 2008; Stoppa *et al.* 2014). RC: Rio Colan (this study); Prd-Mrm: Predazzo–Marmolada (Casetta *et al.* 2019; De Min *et al.* 2020); VF: Val Fiscalina and CB: Corvara in Badia (Lucchini *et al.* 1983); Cc: Calceranica (Galassi *et al.* 1994); WA: Western Alps (Owen, 2008); STALs: Southern Tuscany Alkaline Lamprophyres (Stoppa *et al.* 2014); Tu: Tuscany and MA: Murcia–Almeira (Casalini *et al.* 2022 and references therein); LQ: La Queglia (Vichi *et al.* 2022); PN: Pietre Nere (Bigazzi *et al.* 1996); NF: Nuraxi–Figus (Maccioni & Marchi, 1994). Age references as reported in the text. (b) Simplified map showing the geological domains and major tectonic lines of the northeastern Southern Alps (after Bressan *et al.* 2013, 2018): 1. Quaternary deposits; 2. outer Dinaric domain; 3. Maastrichtian to Upper Carboniferous eastern Southern Alps domain; 4. Palaeocarnic Chain; 5. transcurrent faults; 6. major thrust faults. The red square indicates the location of the Rio Colan dykes. TS: Trieste; GO: Gorizia; UD: Udine; PN: Pordenone. (c) Simplified geological map of the Rio Colan Valley intruded by the Rio Colan olivine minettes (after Carulli *et al.* 1987). Black triangles indicate mountain peaks, with nearby their names and heights in metres.

Despite these mineralogical and geochemical differences, lamproites and lamprophyres are produced through low degrees of partial melting of an extensively depleted peridotite subsequently enriched in incompatible elements. The peridotitic source(s) is expected to be refractory because of the high-Fo olivines, Cr-rich spinels, high whole-rock Mg# (>0.70) and low $Al_2O_3$–CaO–$Na_2O$ contents. In contrast, strong enrichments of large-ion lithophile elements over high-field-strength elements (i.e. high LILE/HFSE ratios) indicate fluids/melts derived by recycling of crustal components and/or carbonatitic metasomatism which results in the formation of phlogopite and/or amphibole-bearing peridotite or veined network (Foley, 1992; Tappe *et al.* 2004, 2006, 2008; Prelević *et al.* 2008, 2010; A Pandey *et al.* 2017*a*, *b*; Fitzpayne *et al.* 2018, 2019; Talukdar *et al.* 2018; R Pandey *et al.* 2019; Choi *et al.* 2020; Casalini *et al.* 2022 and references therein). In the case of highly advanced metasomatism, the primary (i.e. peridotitic) mineralogy can change into a mica–amphibole–rutile–ilmenite–diopside (MARID) assemblage (Foley, 1992; Grégoire *et al.* 2002; Tappe *et al.* 2008; Conticelli *et al.* 2009; Casalini *et al.* 2022 and references therein). Notably, if any of the metasomatic assemblages described above undergoes low degrees (<5 %) of incongruent melting, it can alone reproduce the trace element patterns and isotopic features of lamproites and lamprophyres (and other mafic–ultramafic alkaline rocks like orangeites; Pilet *et al.*, 2008; Tappe *et al.* 2008; Conticelli *et al.* 2009; Giuliani *et al.* 2015; Fitzpayne *et al.* 2018, 2019; Casalini *et al.* 2022).

Lamprophyres and lamproites have been widely recognized along the European margin of the Western Mediterranean Sea (Fig. 1a; Section 2). Most of these mafic to ultramafic alkaline magmas are distributed in space and time over the Italian territory, allowing for a wide investigation of the evolution of the lithospheric and asthenospheric mantle underneath the whole peninsula. In this context, rare and small ultramafic dykes in the Julian Alps (Friuli Venezia Giulia Region; Fig. 1a, b; Carulli *et al.* 1987) can provide clues regarding the geochemical features of the northeasternmost sector of the mantle beneath the Italian peninsula. This work reports on new mineral chemistry, bulk-rock major, and trace elements for these ultramafic intrusions. We show that these magmas are lamprophyres (i.e. olivine minettes) from the mineralogical point of view but geochemically are more akin to lamproites or orangeites. The source of these occurrences underwent extreme depletion and metasomatic processes resulting in geochemical features distinct from the Western Mediterranean lamprophyre and lamproite magmas. Eventually, U–Pb apatite ages obtained via high-spatial-resolution laser ablation – multi-collector – inductively coupled plasma – mass spectrometer (LA-MC-ICP-MS) geochronology were used to constrain the age of these intrusions and frame them in a clear geodynamic context.

## 2. Main features of the Western Mediterranean lamprophyres and lamproites

### 2.a. Lamproites

In the Western Mediterranean area, lamproites crop out (Fig. 1a) in Murcia–Almeria in the Betic zone (~6.4–8.1 Ma; Spain), in northern Corsica (~14.6 Ma; France) and in the Tuscany Region (~0.8–4.2 Ma; Central Italy) (Prelević *et al.* 2008, 2010; Conticelli *et al.* 2009; ages are from Casalini *et al.* 2022 and references therein). Overall, lamproites contain variable amounts of $K_2O$ (3.5–10.7 wt %) and Mg# (0.45–0.87) with Ni and Cr contents up to 849 and 1039 μg/g, respectively. They have high rare earth element (REE) contents, high LILE/HFSE ratios and show a marked positive Pb anomaly in the primitive-normalized (PM) diagrams. They are characterized by high Rb/Sr and low Ba/Rb ratios and a positive correlation between Th/La and Sm/La (Tommasini *et al.* 2011). These features, coupled with crustal Sr, Nd and Pb isotopic compositions, imply derivation from the partial melting of a depleted peridotitic lithospheric mantle cross-cut by lawsonite- (i.e. high Th/La and Sm/La component; Tommasini *et al.* 2011) and phlogopite-bearing (i.e. K-rich) veins which formed during two temporally different events of crustal metasomatism (i.e. vein-plus-wall-rock melting; Foley, 1992; Casalini *et al.* 2022 and references therein).

### 2.b. Lamprophyres

The oldest lamprophyres in Italy crop out at Predazzo and Marmolada (NE Alps; Fig. 1a) and represent the oldest alkaline intrusions in Italy (218–220 Ma, Casetta *et al.* 2019; De Min *et al.* 2020 and references therein). They have a general potassic affinity ($K_2O$ up to ~4 wt %), variable Mg# (0.30–0.70), Ni (27–237 μg/g) and Cr (14–585 μg/g), and have high light REE (LREE) over heavy REE (HREE) ratios. They do not show enrichment in LILEs and PM-normalized multi-element diagrams, lack Ti and Nb troughs and show negative Pb anomalies. Except for a few occurrences displaying high degrees of fractional crystallization and crustal contamination, Sr, Nd and Pb isotopes of the lamprophyres approach the mid-ocean ridge basalt (MORB) values (Casetta *et al.* 2019; De Min *et al.* 2020), and it is generally agreed that they derive from the partial melting of phlogopite + amphibole-bearing spinel ± garnet lherzolite (Casetta *et al.* 2019, 2021; De Min *et al.* 2020). However, whether these alkaline magmas represent a deep mantle section metasomatized during the Variscan orogeny or the transition towards a mantle source progressively exhausting its Varsican imprinting is still debated (see discussion in De Min *et al.* 2020). In addition, Casetta *et al.* (2019) reported a possibility of asthenospheric and carbonatitic components during this alkaline magmatism.

The other lamprophyre occurrences span from the Lower Cretaceous to the Oligocene and are localized (Fig. 1a) in the Western Alps (Sesia Lanzo: ~33–30 Ma (Owen, 2008; see Casalini *et al.* 2022 and references therein for another interpretation)), NE Alps (Calceranica: ~71 Ma (Galassi *et al.* 1994); Corvara in Badia: ~68–70 Ma; Val Fiscalina: ~34 Ma (Lucchini *et al.* 1983)), Tuscany (Southern Tuscany Alkaline lamprophyres: ~90–110 Ma (Vichi *et al.* 2005; Stoppa, 2008; Stoppa *et al.* 2014)), Abruzzo (La Queglia: ~54 Ma (Vichi *et al.* 2022)), Puglia (Pietre Nere: ~58–62 Ma (Bigazzi *et al.* 1996)) and Southern Sardinia regions (Nuraxi Figus: ~60–62 Ma (Maccioni & Marchi, 1994)). These magmas are mafic to ultramafic, alkaline and often carbonatitic (Vichi *et al.* 2005, 2022; Stoppa, 2008 and references therein; Avanzinelli *et al.* 2012; Stoppa *et al.* 2014; Mazzeo *et al.* 2018). They are sodic (mol. % $K_2O/Na_2O < 1$) to ultrapotassic (mol. $K_2O/Na_2O$ ~ 7) with generally high Mg# (0.50–0.91), Ni and Cr (up to 577 and 720 μg/g, respectively), implying they are overall primitive melts. They have high LREE/HREE ratios and show variable enrichments in HFSEs over LILEs. In PM diagrams, Nb, Ta and Ti do not show appreciable negative anomalies, while Pb is more variable, showing marked troughs and slightly positive anomalies (Lucchini *et al.* 1983; Galassi *et al.* 1994; Vichi *et al.* 2005; Bianchini *et al.* 2008; Stoppa, 2008; Conticelli *et al.* 2009; Avanzinelli *et al.* 2012; Stoppa *et al.* 2014; Mazzeo *et al.* 2018). The lamprophyres of the Western Alps and Corvara in Badia are somewhat distinct because they show enrichments in Ba, Th, U, La and Ce and are marked by positive Pb anomalies in PM diagrams, similar to lamproites (Lucchini *et al.* 1983; Peccerillo & Martinotti, 2006; Owen, 2008; Stoppa, 2008; Casalini *et al.* 2022). Concerning the Sr, Nd and Pb isotopic compositions, the lamprophyres cover the range encompassing the DMM, HIMU, FOZO and ITEM (Italian End Member reservoir), pointing towards the EMI and EMII mantle reservoirs (Bianchini *et al.* 2008; Stoppa, 2008; Conticelli *et al.* 2009; Avanzinelli *et al.* 2012; Stoppa *et al.* 2014; Mazzeo *et al.* 2018; Vichi *et al.* 2022). It is suggested that these magmas derive either from an asthenospheric source (FOZO-like) metasomatized by alkaline carbonatitic agents and another LILE- and volatile-rich reservoir (i.e. ITEM; Owen 2008; Stoppa, 2008; Stoppa *et al.* 2014), or, as for the Pietre Nere and La Queglia lamprophyres, from low degrees (~3.5–5 %) of partial melting of non-veined spinel- to garnet-peridotite source metasomatized by Na-rich HIMU components and low in $k$ ($^{232}Th/^{238}U$) (Bianchini *et al.* 2008; Avanzinelli *et al.* 2012; Mazzeo *et al.* 2018; Vichi *et al.* 2022). Additionally, Avanzinelli *et al.* (2012) indicate that these lamprophyres might also have interacted with a component from the sub-continental lithospheric mantle having radiogenic Sr.

## 3. Geological background

The Friuli Venezia Giulia region hosts the easternmost portion of the Italian Alps where three chains are sealed together (Fig. 1b; Bressan *et al.* 2003, 2018; Carulli, 2006; Ponton, 2010). To the north, the weakly metamorphosed Upper Ordovician to Upper Carboniferous turbiditic sequences with overall NW–SE and NE–SW Variscan structures form the Palaeocarnic Chain. The eastern Southern Alps represent the central part and consist of Upper Carboniferous to Maastrichtian carbonates and volcanoclastic sedimentary sequences. The outer Dinarides to the east comprise the Upper Maastrichtian to Miocene flysch and molasse-related sediments. The eastern Southern Alps and outer Dinarides chains developed from the Upper Cretaceous to the Quaternary period following the Adria microplate indentation with the Eurasian plate (e.g. Bressan *et al.* 2003, 2018). Nonetheless, these orogenic processes only partially overprint the Middle Triassic and younger tectonic structures (Ponton, 2010).

To the north of the eastern Southern Alps domain, within the Julian Alps, in the Rio Colan Valley (north of Aupa Valley; Fig. 1b), a few mafic dykes (up to 60 cm wide) crop out in a small area mainly encompassing the Upper Carnian to Upper Norian Monticello Member and Dolomia Principale Formation (Fig. 1c). The area is affected by major NNE–SSW Dinaric-related dextral faults and minor NW–SE and N–S Dinaric-related faults and fractures (Carulli *et al.* 1987). These lineaments are linked

to the Meso- and Neoalpine orogenic stages, with some of them likely inherited from older extensional episodes (Carulli *et al.* 2003; Ponton, 2010). The mafic dykes cross-cut the thick (250–500 m) Monticello Member (Fig. 2a) deposited between the Upper Carnian and Lower Norian. This member consists of stratified grey dolostones with marl intercalations (Carulli *et al.* 1987; Carulli, 2006; Zanferrari *et al.* 2013).

## 4. Methods

Among four sampled dykes in the Rio Colan Valley near the Cuel Brusat Mountain (Fig. 1c), two were carefully selected for mineral chemical, geochemical and geochronological analyses. Due to the narrow width of the intrusions, six samples were collected from the central part and along the length of each dyke. RC1 (i.e. Rio Colan) to RC3 are from dyke 1, and RC4 to RC6 from dyke 2. RC1, RC2, RC3, RC4 and RC5 were selected for the petrographic and mineral chemical screening. Geochemical analyses were performed on RC2, RC3, RC4 and RC5 samples. Alteration products and secondary minerals were carefully removed using an optical microscope prior to sample preparation for geochemical analyses. Mineral chemical compositions were determined at the Department of Geoscience of the University of Padova, Italy. Whole-rock major and trace elements were analysed at the Department of Geoscience, University of Padua, Italy, and ACME Labs (Vancouver, Canada), respectively.

Samples RC2 and RC5 from dykes 1 and 2, respectively, were further selected to separate apatite crystals for U–Pb geochronology and apatite major element analyses. For both samples, clinopyroxenes were also separated to analyse their apatite inclusions. Apatite and clinopyroxene separation procedures, backscattered electron image (BSE), cathodoluminescence (CL) images and U–Pb dating were performed at the Microscopy and Microanalysis Laboratory (LMic) and Applied Isotope Research Group (AIR-G) of the Department of Geoscience of the Federal University of Ouro Preto, Brazil, following procedures in Lana *et al.* (2017, 2021). Further details on the methodologies adopted (Online Supplementary Materials) and tables (Online Supplementary Tables S1 to S4) are available at https://doi.org/10.1017/S0016756823000183.

## 5. Results

### 5.a. Field and petrographic relationships

Dykes are up to 60 cm wide (Fig. 2a) and cut only the local observable upper Triassic sequence. Their length cannot be assessed because they appear as columns of a few tens of metres along a sub-vertical rock face. They are discordant with respect to the stratification of the Monticello Member (Fig. 2a), showing a NE–SW orientation similar to some NNE–SSW and N–S (recent?) faults (Fig. 1c). Fractures likely related to Alpine deformations were also recognized. No crustal xenoliths are visible at the contact with the host rock, but possible crustal contamination will be discussed further below.

Rocks are dominated by abundant phenocrysts of olivine, biotite–phlogopite and clinopyroxenes (Fig. 2b–f). Only olivines are serpentinized and form ~0.5 to ~1.5 mm sized euhedral to subeuhedral crystals (Fig. 2b–d). Biotite–phlogopites form principally laths (up to ~1 mm in length; Fig. 2b, c) and, occasionally, euhedral hexagonal plats (up to ~0.2 mm in diameter; Fig. 2f). Micas are occasionally rimmed by tetraferriphlogopite. Clinopyroxenes are elongated (from ~0.2 to ~0.5 mm in length), sub-euhedral and slightly zoned (Fig. 2b, d, e). The same minerals that form phenocrysts also form the groundmass and are immersed in a holocrystalline to ialocrystalline matrix with an intergranular texture (Fig. 2b–f). Apatite crystals are the most abundant primary accessory minerals and are frequently found as needles in the groundmass or as inclusions in micas and clinopyroxenes (Fig. 2f). In clinopyroxenes, apatite crystals are not always associated with fracture (Fig. 2e) which excludes them from being of secondary origin. Since apatites are included in micas and clinopyroxenes but not in altered olivines, olivines were the first to crystallize, followed by apatites, micas and clinopyroxenes. Other primary minerals are chromites, also included in serpentinized olivines (Fig. 2c, d), and in lesser amounts magnetites. Secondary phases (i.e. carbonate-filling vacuoles, zeolites substituting glassy patches and/or foids, and albite) are rare.

### 5.b. Mineral chemistry

Clinopyroxenes have homogeneous diopsidic composition ($Wo_{46–55}En_{30–46}Fs_{6–21}$; Online Supplementary Table S2) being consistent with those documented in worldwide potassic-alkaline magmatic suites such as Asunción –Sapucai Graben (Cundari & Comin-Chiaramonti, 1996) and Roman Province (Cundari & Ferguson, 1982) (Fig. 3a). Furthermore, Rio Colan clinopyroxenes plot above the Si + Al = 2 line (Fig. S1 in Online Supplementary Figures) corresponding to the full occupancy of Si and Al in the tetrahedral site. Consequently, a small amount of Al in the octahedral site is also present as $Al^{VI}$. Ti vs $Al_{Tot}$ (Fig. 3b) shows a positive relationship with clinopyroxenes plotting between the lamproite-transitional fields represented by the clinopyroxenes derived from mica-rich lamprophyres (i.e. minette) (Mitchell & Bergman, 1991; Lustrino *et al.* 2016).

Micas are classified as biotite–phlogopites (Fig. 4a), with the Mg# ranging from 0.59 to 0.78 (Online Supplementary Table S2). Indeed, $Al_2O_3$ is high and similar between cores and rims around 15–16 wt %. $TiO_2$ shows similar behaviour to that seen for $Al_2O_3$, while $FeO_{Tot}$ is more enriched in the rims (11.40 to 16.81 wt %) than in the cores (9.06–12.87 wt %). In Fig. 4b ($Al_2O_3$ vs $TiO_2$), micas plot at the limit between the minettes and kimberlite fields (Mitchell, 1995; Chalapathi Rao *et al.* 2004), whereas with regard to $FeO_{Tot}$ (Fig. 4c), the crystals plot along with the minette/ultramafic lamprophyre trend (Mitchell, 1995; Tappe *et al.* 2004).

The chemical formula and OH contents of apatites were recalculated using Ketcham (2015) workflow (Online Supplementary Table S2). Handpicked apatites have low F (0.34–0.69 atom per formula unit (apfu)) and Cl (0.23–0.30 apfu) but high OH (1.04–1.43 apfu) contents. This classifies apatites as hydroxylapatite (Fig. 5a) because of their low F/OH and Cl/OH ratios (0.24–0.66 and 0.16–0.28, respectively). Apatite crystals included in clinopyroxenes are also hydroxylapatites ($F = 0.42–0.79$ apfu; $Cl = 0.23–0.32$ apfu; $OH = 0.89–1.35$ apfu; $F/OH = 0.31–0.89$; $Cl/OH = 0.17–0.23$). Note that all apatite crystals tend to have more F than Cl ($F/Cl = 1.48–2.77$). In addition, apatites show $P_2O_5$ (40.06–40.98 wt %) and SrO (0.09–0.25 wt %) contents comparable to similar crystals from calc-alkaline and ultramafic on-craton lamprophyres (Dalton *et al.* 2019; Choi *et al.* 2020; Soltys *et al.* 2020), worldwide on-craton orangeites, on-craton kimberlites and carbonatites (data from Soltys *et al.* 2020). Rio Colan apatites plot outside the area of worldwide lamproites (i.e. Soltys *et al.* 2020) and show much lower SrO contents compared to other Italian

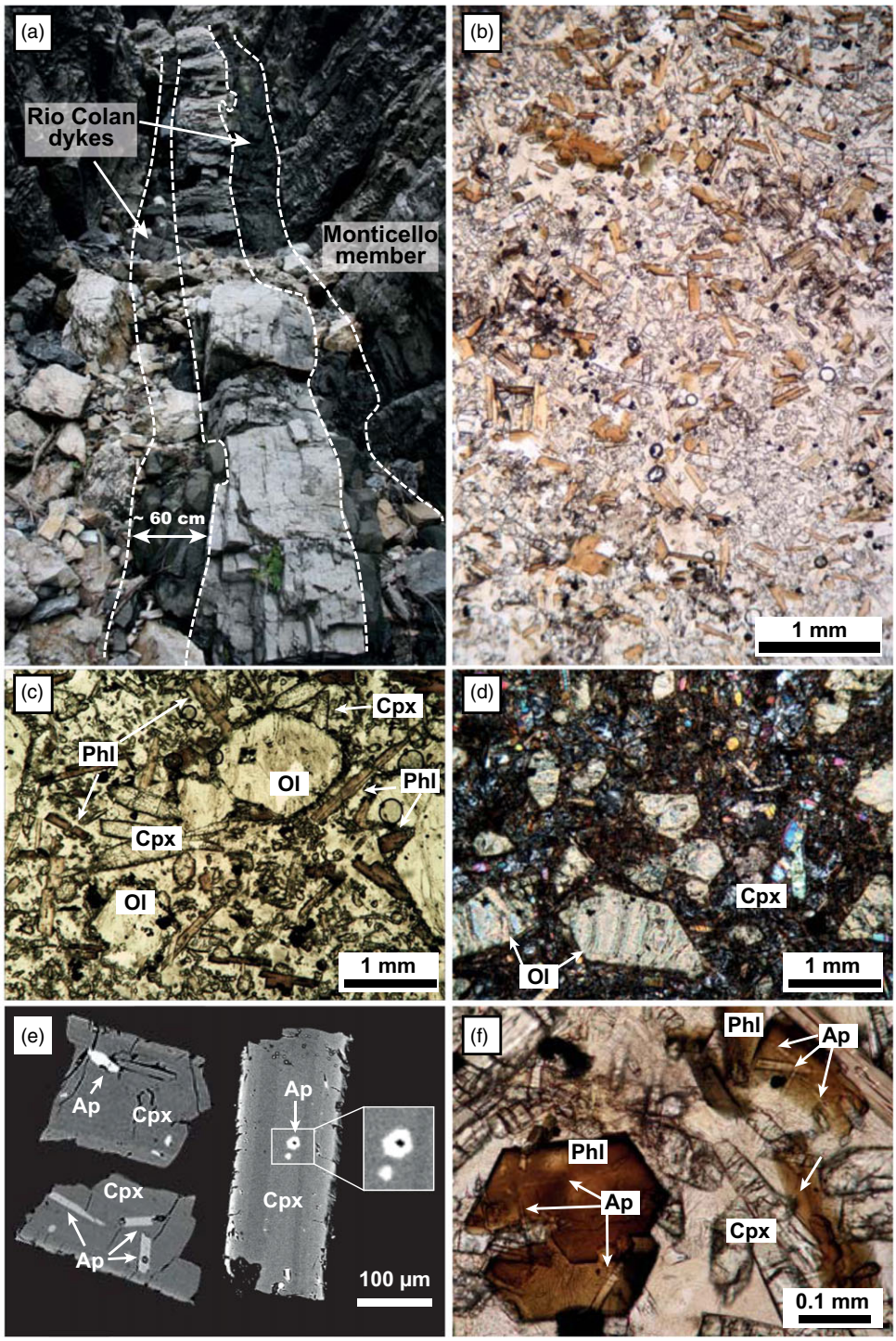


**Fig. 2.** (Colour online) (a) Example of Rio Colan dykes in the field. Note the lack of interaction with the wall rock and the absence of crustal xenoliths. (b, c) Phenocrysts of serpentinized olivines, biotites–phlogopites and clinopyroxene within a holocrystalline to ialocrystalline matrix with intergranular texture. Light brown groundmass represents zeolitized glass. (b) and (c) are high- and low-Mg olivine minette dykes, respectively. (d) Serpentinized olivine due to autohydrothermalism. Note that the matrix and other minerals do not show hydrothermal alteration. (e) Backscattered image of clinopyroxenes with apatite inclusions. Note that not all apatites are linked to fractures. (f) Apatite inclusions in biotite–phlogopite crystals of the high-Mg olivine minette in (b). Note that (f) is a zoom into a portion outside the area reported in (b).

lamprophyres (Stoppa, 2008; Stoppa *et al.* 2014). Note that the apatites from Italian lamprophyres have composition indistinguishable from other mafic–ultramafic on–off craton rocks.

Spinels are all magnesio-chromites [Cr# (Cr/Cr + Al) = 0.70–0.78; Mg# (Mg/Mg + $Fe^{2+}$) = 0.42–0.55], with low $Fe^{2+}/Fe^{3+}$ ratio (1.51–3.27), and relatively high $TiO_2$ (0.52–1.38 wt %) and $Al_2O_3$ (10.12–12.18 wt %) except for one grain (Online Supplementary Table S2). These values would resemble those of magmatic spinels found in kimberlites and arc to alkaline–carbonate-rich magmas. Two oxides were also analysed and classified as Ti-magnetites ($TiO_2$ = 5.17–5.26 wt %; $FeO_{Tot}$ = 80.22–82.61 wt %). Eventually, the few analyses on groundmass feldspar grains classify them as $FeO_{Tot}$-poor ($FeO_{Tot}$ = 0.24–0.69) orthoclase ($Or_{53–78}Ab_{18–35}An_{1–12}$).

### 5.c. LA-MC-ICP-MS U–Pb apatite ages

Handpicked apatite crystals under CL show euhedral to sub-euhedral stubby and prismatic shapes with a wide range of length:width ratios (0.5:1 < L:W < 2:2; Fig. 6a). Almost all the crystals have diameters ≤50 µm. The grains are fracture-free and show a core-to-rim magmatic oscillatory zoning. For RC2 and RC5 dykes,

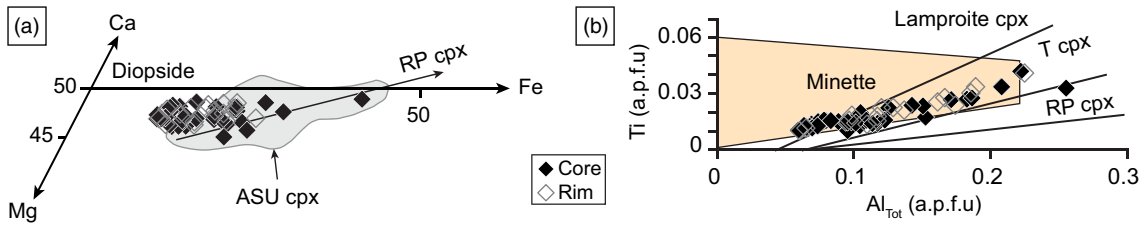


**Fig. 3.** (Colour online) Clinopyroxenes classification. (a) Ca–Mg–Fe pyroxene classification diagram. RP cpx: Roman Province clinopyroxene from Cundari and Ferguson (1982); ASU cpx: Asunción–Sapucai Graben clinopyroxene from Cundari and Comin-Chiaramonti (1996). (b) Ti vs At$_{Tot}$ for the Rio Colan clinopyroxenes (modified after Mitchell, 1995; Lustrino *et al.* 2016). Minette field from Mitchell (1995). T cpx: transitional clinopyroxenes from Lustino *et al.* (2016 and references therein).

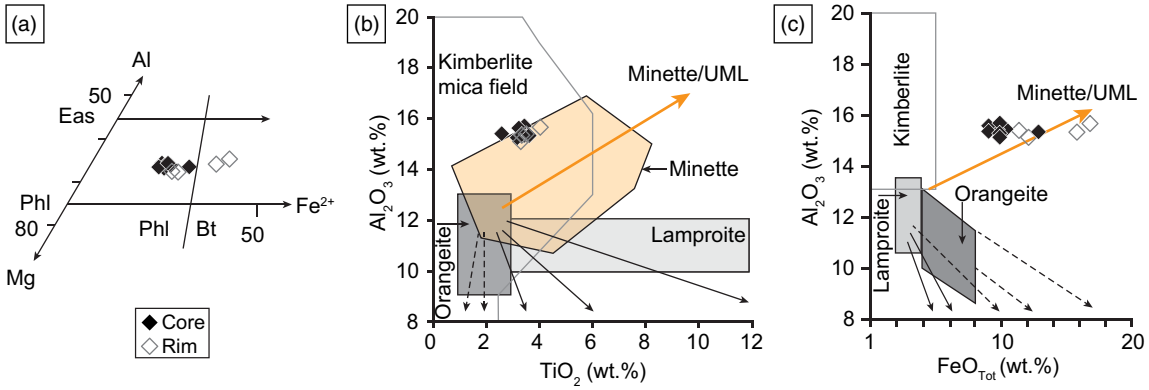


**Fig. 4.** (Colour online) Micas classification. (a) Mg–Al–Fe$^{2+}$ diagram and (b) $TiO_2$ vs $Al_2O_3$ and (c) $FeO_{Tot}$ vs $Al_2O_3$ diagrams (in wt %) for the Rio Colan micas. Diagrams modified from Mitchell (1995), Chalapathi Rao *et al.* (2004) and Tappe *et al.* (2004).

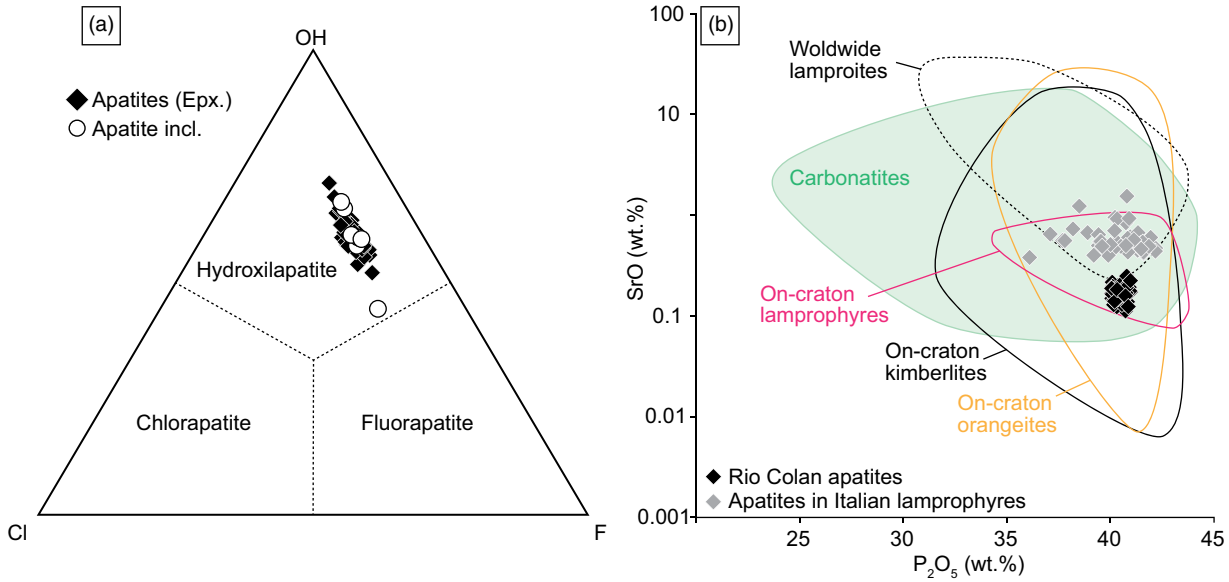


**Fig. 5.** (Colour online) (a) Apatites classification based on the Cl–F–OH diagram (after Patiño Douce *et al.* 2011). Epx.: apatites mounted in epoxy resin and analysed before dating; incl.: apatites included in clinopyroxenes of Figure 2e. (b) $P_2O_5$ (wt %) vs SrO (wt %) diagram of apatites in mafic–ultramafic alkaline magmas. Apatites in Italian lamprophyres: Stoppa (2008) and Stoppa *et al.* (2014). Apatites in on-craton lamprophyres: Choi *et al.* (2020), Dalton *et al.* (2019) and Soltys *et al.* (2020). Apatite in lamproites, orangeites, kimberlites and carbonatites are from Soltys *et al.* (2020).

only 15 and 23 U–Pb apatite dates were suitable for the Tera–Wasserburg concordia diagram. Analyses are presented without correction for common Pb. Except for a few grains in RC5 (Fig. 6b), all remaining apatites have not developed enough spread in common Pb / radiogenic Pb (Fig. 6b), which would have resulted in a linear array on the concordia diagram (Chew *et al.* 2011). Other low-U co-genetic minerals with very low in-growth radiogenic Pb were not analysed because they were absent (e.g. titanite) or rare and too small (e.g. feldspar). Therefore, to obtain the initial Pb composition, we used the same strategy adopted by Chew *et al.* (2011 and references therein), Pochon *et al.* (2016) and Lana *et al.* (2021). On the Tera–Wasserburg diagram, we firstly projected the

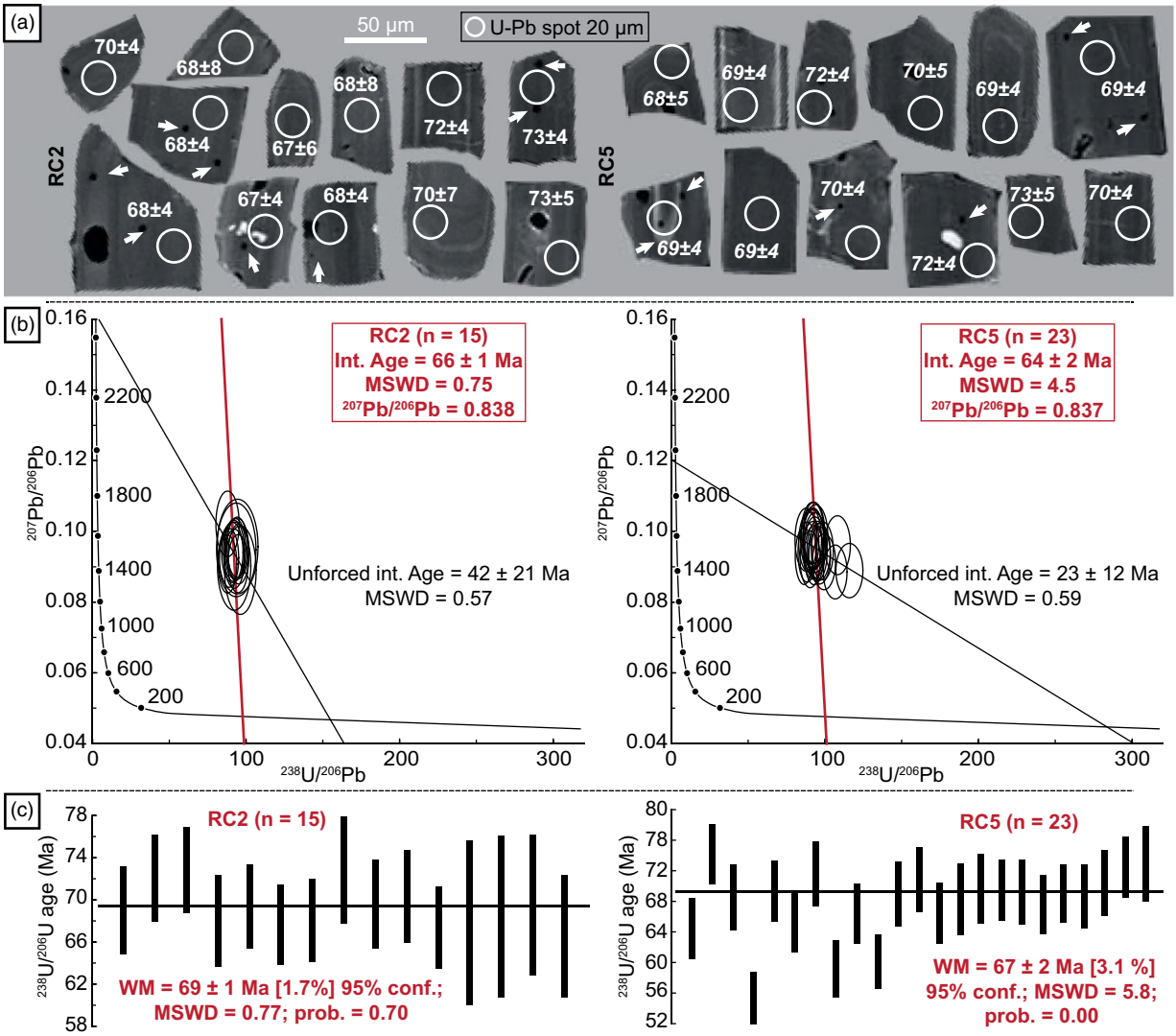


**Fig. 6.** (Colour online) Apatites cathodoluminescence and geochronology. (a) CL images of the apatite crystals dated from the RC2 and RC5 dykes. White arrows indicate electron microprobe analyser (EMPA) spot analyses whose results are reported in Figure 5. Ages near the spots are $^{206}Pb/^{238}U$ weighted mean ages showing good age agreement despite some spots ablated zoned parts of the apatites. (b) Tera–Wasserburg concordia diagrams and (c) $^{206}Pb/^{238}U$ weighted mean ages of the Rio Colan apatites.

unforced discordia (black line in Fig. 6b) to obtain a lower intercept date (*x*-axes) to calculate the initial $^{207}Pb/^{206}Pb$ using the two-stage terrestrial Pb evolution model of Stacey and Kramers, (1975). Afterwards, the data were plotted again to construct a discordia anchored (red line) to the estimated $^{207}Pb/^{206}Pb$ from the evolution model. For the RC2 sample, the unforced lower intercept gives a date of 42 ± 21 Ma (2SE; MSWD = 0.56) identical, within the error, with the unforced discordia of RC5 dyke (23 ± 12 Ma 2SE; MSDW = 0.59). Once both ages are anchored to an estimated $^{207}Pb/^{206}Pb$ ratio of 0.838 for RC2 and 0.387 for RC5, the resulting forced discordia ages were 66 ± 1 Ma (2SE; MSDW = 0.75) and 64 ± 2 Ma (2SE; MSWD = 4.5) for RC5 and RC2, respectively (Fig. 6b). It is worth reporting that some spots (Fig. 6a) appear to have ablated zoned domains of the apatite grains. However, all but three weighted mean ages are consistent with each other, which excludes any mixed age (Fig. 6c). In this regard, the $^{207}Pb/^{238}U$ weighted average date for RC2 is 69 ± 1 Ma (2SE; MSWD = 0.77; $n = 15$) which is, considering the error, only 1 Ma older than the anchored age, and up to ~30 Ma older than the unforced age. Conversely, the $^{207}Pb/^{238}U$ weighted average date of RC5 is 67 ± 2 Ma (2SE; MSWD = 5.8; $n = 23$), which is identical within the error with forced age, yet older by ~45 Ma than the unforced age.

### 5.d. Whole-rock geochemistry

In the mafic–felsic-weathering (MFW) (Fig. S2 in Online Supplementary Figures) of Ohta and Arai (2007), all whole-rock analyses show a weathering index W well below 30 % of the cut-off line diagram, indicating dykes 1 and 2 had negligible element mobility. Therefore, for each dyke, we used the averaged whole-rock analyses (Online Supplementary Table S1). The most striking difference between dykes 1 and 2 is the different MgO content (11.9 and 16.7 wt %, respectively) corresponding to an Mg# of 0.73 and 0.79 (for an assumed $Fe_2O_3/FeO = 0.20$), respectively. Dyke 1 with low Mg# (Rio Colan LMg#) shows Cr and Ni contents (862 and 198 μg/g, respectively) lower than those displayed by dyke 2 high in Mg# (Rio Colan HMg#; Cr and Ni = 1416 and 360 μg/g, respectively). Figure 7a reports the sum of these minor compatible elements against the relative MgO content of both dykes to

highlight these features better. Rio Colan LMg# dyke is Ne-normative, has $K_2O + Na_2O = 5.8$ wt %, an agpaitic index (AI = (K + Na)/Al) mol.%) = of 0.54 and $K_2O/Al_2O_3$ of 0.37 (mol. %). Rio Colan HMg# is Ol- and Hy-normative, has $K_2O + Na_2O = 4.1$ wt %, with A.I = 0.44 and $K_2O/Al_2O_3$ of 0.32 (mol. %). Nevertheless, Rio Colan LMg# and HMg# dykes show nearly similar high $K_2O$ (3.3–4.4 wt %), CaO (8.2–9.6 wt %), $Al_2O_3$ (11–13 wt %) and $TiO_2$ (1.07–1.13 wt %) contents (Fig. 7b–d). Both dykes display high abundances in Ba (3452–3974 μg/g) and La (113–135 μg/g), while Zr and Sr are relatively low (112–139 and 362–549 μg/g, respectively; Online Supplementary Table S1).

Chondrite-normalized diagrams (CN; recommended chondrite; Boynton 1984) and primitive-mantle-normalized spider plots (PM; McDonough & Sun, 1995) are reported in Figures 8 and 9, respectively. Both Rio Colan LMg# and HMg# dykes show similar REE patterns as seen by the relatively uniform $La/Yb_{CN}$ (42–49), $La/Ce_{CN}$ (~2.2) $La/Sm_{CN}$ (14–15), $Sm/Dy_{CN}$ (2.5–2.7), $Dy/Yb_{CN}$ (1.1–1.3) and Eu/Eu* (0.85–0.93) ratios (Fig. 8a). These ratios indicate LREE enrichment over MREE and HREEs with a negligible Eu negative anomaly. Such homogeneity is also seen for the incompatible elements, with both dykes showing, in addition to high Ba, Th and U abundances, positive anomalies in Nb ($La/Nb_{PM} = 1.4$) and P ($P/Nd_{PM} = 1.9$–2.2) while no anomaly in Pb is detected (Fig. 9a).

## 6. Discussions

### 6.a. Classification of the Rio Colan dykes

Rio Colan dykes show the preservation of equilibrium of phenocrysts of olivine + biotite–phlogopite + diopside + apatite ± opaques. This equilibrium implies these are mafic minettes, that is, primitive magmas (or primitive minettes) (Esperança & Holloway, 1987; O'Brien *et al.* 1991; Tingey *et al.* 1991; Canning *et al.* 1996; Righter & Carmichael, 1996; Rukhlov *et al.* 2013), in agreement with their high Mg# (0.7 and 0.8), Cr (862 to 1416 μg/g) and Ni (198 to 360 μg/g). According to Esperança and Holloway (1987), the preservation of such mineralogical equilibrium indicates magmas were brought to the surface rapidly at ~1000–1200 °C, a process that also precludes fractionation at lower pressure and temperatures (Esperança & Holloway, 1987). This could explain the absence of plagioclase as it would have hampered it from nucleating in the groundmass. Furthermore, Rio Colan olivine minettes have LOI (loss-on-ignition) of 7–8, suggesting high content of volatiles ($H_2O$ and $CO_2$), as also supported by the great abundance of hydroxylapatites (Fig. 5a). We argue that this would have suppressed plagioclase, enhancing biotite–phlogopite and diopside precipitation (e.g. Carmichael *et al.* 1996), and caused olivine autohydrothermalism (e.g. Tingey *et al.* 1991).

Low agpaitic index, low molar K/Al ratio and the Ol- to Ne-normative character for the Rio Colan dykes would further support that these magmas are lamprophyres. The excess of Al in the clinopyroxene octahedral site (Fig. 3b), the high $Al_2O_3$ and $FeO_{Tot}$ and low $TiO_2$ in biotite–phlogopites (Fig. 4b, c) and $FeO_{Tot}$-poor orthoclases support that the dykes are minette. Likewise, since apatites were among the first minerals to crystallize, their chemistry reflects the nature of the magma. According to their chemistry, Rio Colan LMg# and HMg# magmas are more similar to lamprophyres than lamproites (Fig. 5b). High MgO, Cr, Ni (Cr + Ni), $K_2O$ and $Al_2O_3$ coupled with low CaO and NaO contents are possible features among lamprophyric magmas (Fig. 7a, b, d), in particular primitive alkaline magmas (Esperança & Holloway, 1987; O'Brien *et al.* 1991; Tingey *et al.* 1991; Canning *et al.* 1996; Righter & Carmichael, 1996; Stoppa, 2008; Tappe *et al.* 2008; Rukhlov *et al.* 2013; Stoppa *et al.* 2014). However, in Rio Colan olivine minettes, LREE, LILEs (except for Pb) and HFSE variations are in between those reported for Corvara in Badia, Val Fiscalina, Calceranica, La Queglia and Pietre Nere lamprophyres, and to a lesser extent mirror the Western Alps minettes (Figs 8a–c, 9a–c; Bianchini *et al.* 2008; Owen, 2008; Stoppa, 2008; Conticelli *et al.* 2009; Avanzinelli *et al.* 2012; Mazzeo *et al.* 2018). Less evident is a similarity with Southern Tuscany Alkaline Lamprophyres (STALs) and Predazzo–Marmolada counterparts (Figs 8a, b, and 9a, b; Stoppa *et al.* 2014; Casetta *et al.* 2019; De Min *et al.* 2020). On the other hand, major, minor and incompatible elements variations in Rio Colan olivine minettes also resemble those found in Tuscan, Sisco and Murcia–Almeria lamproites (Prelević *et al.* 2008, 2010; Conticelli *et al.* 2009; Casalini *et al.* 2022). This is particularly evident considering the major element variation (Fig. 7) and the low Ti, Zr and Sr coupled with high Ba, Th, U and La concentrations (Fig. 9). Pb is less abundant and shows no anomaly with respect to lamproite magmas. We therefore argue that while Rio Colan magmas are olivine minettes from the petrographic and mineral chemistry point of view, their geochemical signature shares affinities with lamprophyres and lamproites.

### 6.b. Petrogenetic aspects

Rio Colan olivine minettes are one of the most primitive magmas among the Western Mediterranean lamprophyres and lamproites (Fig. 7a). The high MgO and Cr + Ni contents coupled with a low $Dy/Yb_{CN}$ and flat HREE pattern (Fig. 8a) suggest that Rio Colan olivine minettes were derived from a depleted peridotitic source that underwent very low degrees of partial melting in the presence of possible residual olivine and garnet (e.g. Becker & Le Roex, 2007). On the other hand, high $K_2O$ content, high $La/Sm_{CN}$ ratios, and LILE enrichments (Figs 7b, 8a, 9a, respectively) indicate that this depleted peridotitic source had been hydrated and enriched in incompatible elements prior to the melting event (Foley *et al.* 1987; Tappe *et al.* 2006, 2008; Conticelli *et al.* 2009; Prelević *et al.* 2010; Stoppa *et al.* 2014; Fitzpayne *et al.* 2018, 2019 and references therein; Lustrino *et al.* 2016). However, it is unlikely that the recycling of oceanic crustal material triggered such metasomatism, given the lack of any positive Pb anomaly in the Rio Colan olivine minettes. Low Nb/U but high Nb (Fig. 10a) would argue against sediment-derived metasomatism, yet this is challenged by the ultrapotassic nature of the Rio Colan magmas, and their high Th/Yb (22 to 23; Fig. 11a) and Ba contents. The slightly negative Th anomaly and $Th/U_{PM} < 1$ (0.73–0.80) indicate that crustal metasomatism would have acted in the form of melt(s) rather than fluid(s) (e.g. Conticelli *et al.* 2009). Low Ba/Th (89 to 95) and high $La/Sm_{CN}$ (14.4 to 14.9) ratios support this observation. This enrichment in incompatible elements allowed the precipitation of hydrated minerals in the source region. The Rb/Sr vs Ba/Rb diagram (Fig. 10b) would suggest an equal amount of phlogopite and amphibole, but the lack of amphibole in the Rio Colan olivine minettes would indicate the presence of phlogopite in the source.

In addition, the Rio Colan minettes show superchondritic Nb/Ta ratios, higher than the other lamprophyres and lamproites reported here (Fig. 10c). Only a few Predazzo–Marmolada and STALs lamprophyres show high Nb/Ta ratios. Such high ratios exclude the involvement of amphiboles in the source or as a crystallizing phase because these minerals cannot produce

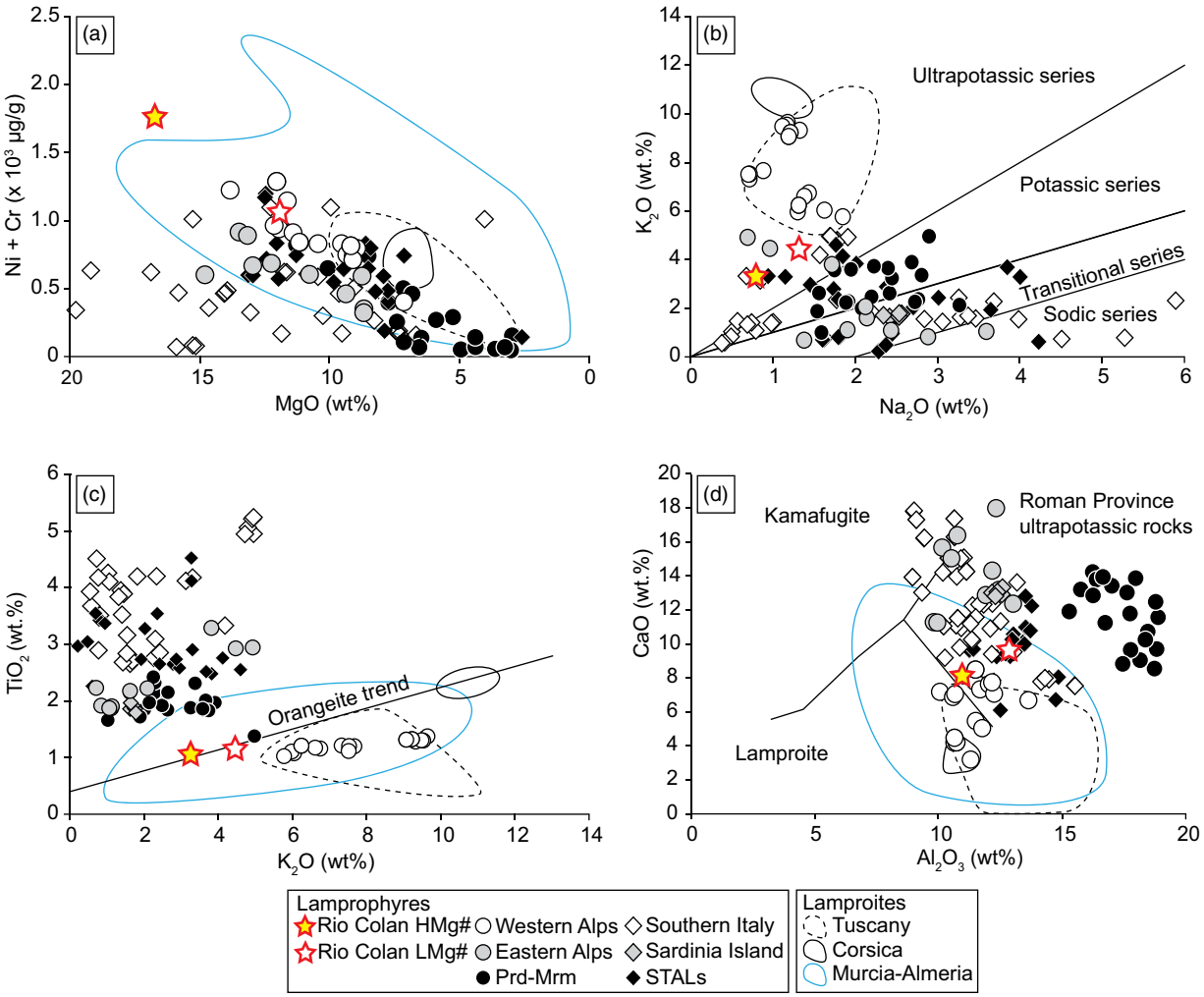


**Fig. 7.** (Colour online) Major (wt %; loss-on-ignition-(LOI)-free basis) and minor elements (µg/g) variation diagrams. (a) MgO vs Ni + Cr, (b) $Na_2O$ vs $K_2O$, (c) $K_2O$ vs $TiO_2$ and (d) $Al_2O_3$ vs CaO. Note that in (a) the Rio Colan olivine minettes are one of the most primitive magmatic products among the lamprophyres and lamproites used for comparison, and in (c) the same rocks plot along with the orangeite trend like other lamproite magmas. Orangeite (i.e. South African group II kimberlites) trend from Becker and Le Roex (2006). (d) modified after Foley *et al.* (1987). Rio Colan HMg# and LMg# indicate Rio Colan dykes showing high and low Mg#, respectively. Lamprophyres: Prd-Mrm (Predazzo–Marmolada): Casetta *et al.* (2019) and De Min *et al.* (2020); Eastern Alps (Corvara in Badia, Val Fiscalina and Calceranica): Lucchini *et al.* (1983), Galassi *et al.* (1994) and Stoppa (2008); Western Alps: Owen (2008), Peccerillo and Martinotti (2006); STALs (Southern Tuscan Alkaline Lamprophyres): Stoppa *et al.* (2014); Southern Italy (La Queglia and Punte Pietre Nere): Bianchini *et al.* (2008), Stoppa (2008), Avanzinelli *et al.* (2012), Mazzeo *et al.* (2018) and Vichi *et al.* (2022); Sardinia Island (Nuraxi Figus): Maccioni & Marchi, 1994) and Stoppa (2008). Lamproites from Tuscany (Italy), Corsica Island (France) and Murcia–Almeira (Spain) are from Conticelli *et al.* (2009), Lustrino *et al.* 2016) and Casalini *et al.* (2022). For the Pietre Nere we used only the less evolved magmas.

superchondritic Nb/Ta ratios (Foley *et al.* 2000, Foley *et al.* 2002; Tiepolo *et al.* 2000; A Pandey *et al.* 2018 and references therein). This is consistent with the lack of this hydrous mineral in the source (Fig. 10b) and in the Rio Colan olivine minettes (Fig. 2b–f). Conversely, because rutile accommodates in its crystalline structure more Nb than Ta (Foley *et al.* 2000, Foley *et al.* 2002), high Nb/Ta ratios can reflect rutile-rich metasomatism (Guo *et al.* 2004; Moayyed *et al.* 2008; A Pandey *et al.* 2018 and references therein; Talukdar *et al.* 2018). For instance, Guo *et al.* (2004) demonstrate that high Nb/Ta in the Sulu orogen lamprophyres might have been derived from a rutile-rich metasomatized source. After carbonatitic metasomatism, the source achieved a superchondritic Nb/Ta ratio when rutile was extracted from an ultra-high-pressure eclogite and dissolved in the melt that metasomatized the mantle (Guo *et al.* 2004). Aulbach *et al.* (2011) provide more constraints on this process, showing that it can be achieved when a mantle source, previously metasomatized by a carbonatitic agent, reacts with a Ti-rich ($TiO_2$ > 2 wt %) ocean island basanite that can fractionate considerable amounts of rutile. According to those authors, in the case of MARID and metasomatized peridotite rocks, rutile must fractionate before the accumulation or addition of phlogopite, rutile, ilmenite and secondary clinopyroxene. Interestingly, by using the same modelling approach, the same geochemical parameters and alkaline–carbonate-rich melt composition (K109 basanite; $TiO_2$ = 2.47 wt %; MgO = 15.5 wt %; Mg# = 0.71; Zr/Hf = 38.9; Nb/Ta = 16.4; Chauvel *et al.* 1992; Pfänder *et al.* 2007) adopted by Aulbach *et al.* (2011; and details therein) it was possible to explain the high Nb/Ta ratio of the Rio Colan LMg# olivine minette (faded orange trend a in Fig. 10c). Note that the Rio Colan HMg# olivine minette can be explained with a Ti-rich alkaline–carbonate-rich melt showing a lower Zr/Hf ratio. However, for our specific case, this alkaline–carbonate-rich melt must have percolated through the source before the intrusion of the Rio Colan magmas, must have been older than the Rio

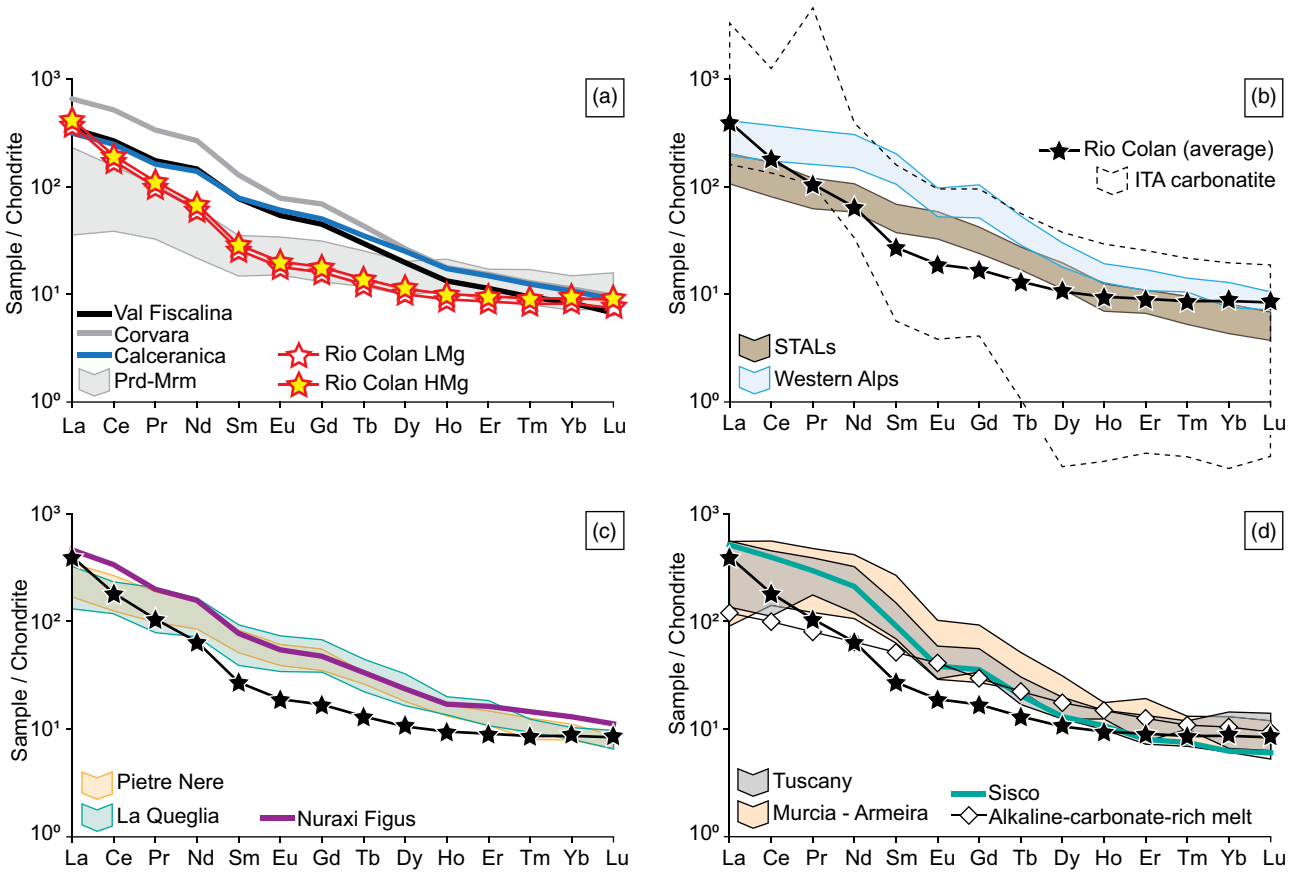


**Fig. 8.** (Colour online) Chondrite-normalized rare earth elements ($REE_{CN}$) patterns for the Rio Colan olivine minettes and the other lamprophyres and lamproites of the Western Mediterranean. From (a) to (d) Rio Colan REEs patterns are compared against those of the Italian lamprophyres and Italian, French and Spanish lamproites. In (b–d), Rio Colan magmas are reported as average. In (b), Italian carbonatitic magmatism is from Stoppa *et al.* (2016, 2019). In (d), alkaline–carbonate-rich melt is from Suns and McDonough (1989). Nuraxi Figus lamprophyres and Sisco lamproites are average values. Data sources as in Figure 7.

Colan dykes (see Section 6.c) and must crop out near the investigated area. In literature, hydrous alkaline magmatism that meets these requirements could be related to the middle- to late-Triassic magmatism of the Karawanken area (Miller *et al.* 2011) and the Italian Dolomites (see Fig. 1a; Casetta *et al.* 2019; De Min *et al.* 2020). Alkaline–carbonate-rich lamprophyres from the Dolomites cannot be used for our modelling because their Zr/Hf ratios are higher than those of the Rio Colan olivine minettes, or their $TiO_2$ and/or Mg# are too low. On the other hand, the alkaline–carbonate-rich melt-like gabbro 08EK18 of the Karawanken area (Miller *et al.* 2011; $TiO_2 = 2.9$ wt %; MgO = 11.7 wt %; Mg# = 70; Zr/Hf = 36; Nb/Ta = 12) is close to the composition of K109 basanite and can explain the superchondritic Nb/Ta ratios of the Rio Colan HMg# dykes after fractionating between 6 and 7 % of rutile (Fig. 10c). Although the trajectory of this modelling would also explain the Nb/Ta value of the Rio Colan LMg# dyke, their different Zr/Hf ratios would imply some dependency on the Zr/Hf ratio of the alkaline–carbonate-rich melt that percolated through the carbonated peridotite. Regardless of this point, this alkaline–carbonate-rich melt-mediated rutile fractionation process (Aulbach *et al.* 2011) explains why Rio Colan magmas are ultrapotassic, low in Nb/U ratio, high in Nb, and, being alkaline–carbonate-rich, melt-like as shown by the Ce/Pb vs Ce diagram (Fig. 10d). We further notice that the Nb/Ta – Zr/Hf ratios of some of the Western Alps, NE Alps, STAL and Southern Italy lamprophyres can be explained through the same modelling involving ~4 % of rutile fractionation (Fig. 10c). This is consistent with the presence of Ti-rich minerals in the source of STALs (Stoppa *et al.* 2014). Notably, Rio Colan olivine minettes and many South African on-craton orangeites share similar superchondritic Nb/Ta ratios (cf. Fig. 10c with fig. 6b in Aulbach *et al.* 2011) and low $TiO_2$ contents (Fig. 7c) as well as apatite compositions (Fig. 5b).

Another alternative expalanation for the high Nb/Ta ratios is the dependence of high Nb contents with respect to the depth of the source and Al solubility in clinopyroxene (e.g. Baier *et al.* 2008; De Min *et al.* 2020). Baier *et al.* (2008) showed that Nb content in clinopyroxene increases as both tetrahedral Al and the pressure increase. However, as Ta and Nb have the same solubility behaviour in clinopyroxene (Baier *et al.* 2008), this would result in magmas with low Nb/Ta ratios, which are not observed here. Eventually, we exclude that these ratios reflect the assimilation of country rocks (i.e. carbonates) because (i) we did not see any evidence of carbonate xenoliths in the field (Fig. 2a), (ii) the mineralogy of the Rio Colan olivine minettes requires a high rate of emplacement and crystallization which prevents any crustal assimilation (Esperança & Holloway, 1987), and (iii) the high LILE contents of the Rio Colan dykes (Fig. 9a) exclude limestone assimilation as this would lower their LILE contents (e.g. Vichi *et al.* 2005).

In summary, our observations imply a depleted peridotitic source(s) that reacted with fluids/melts derived by recycling of

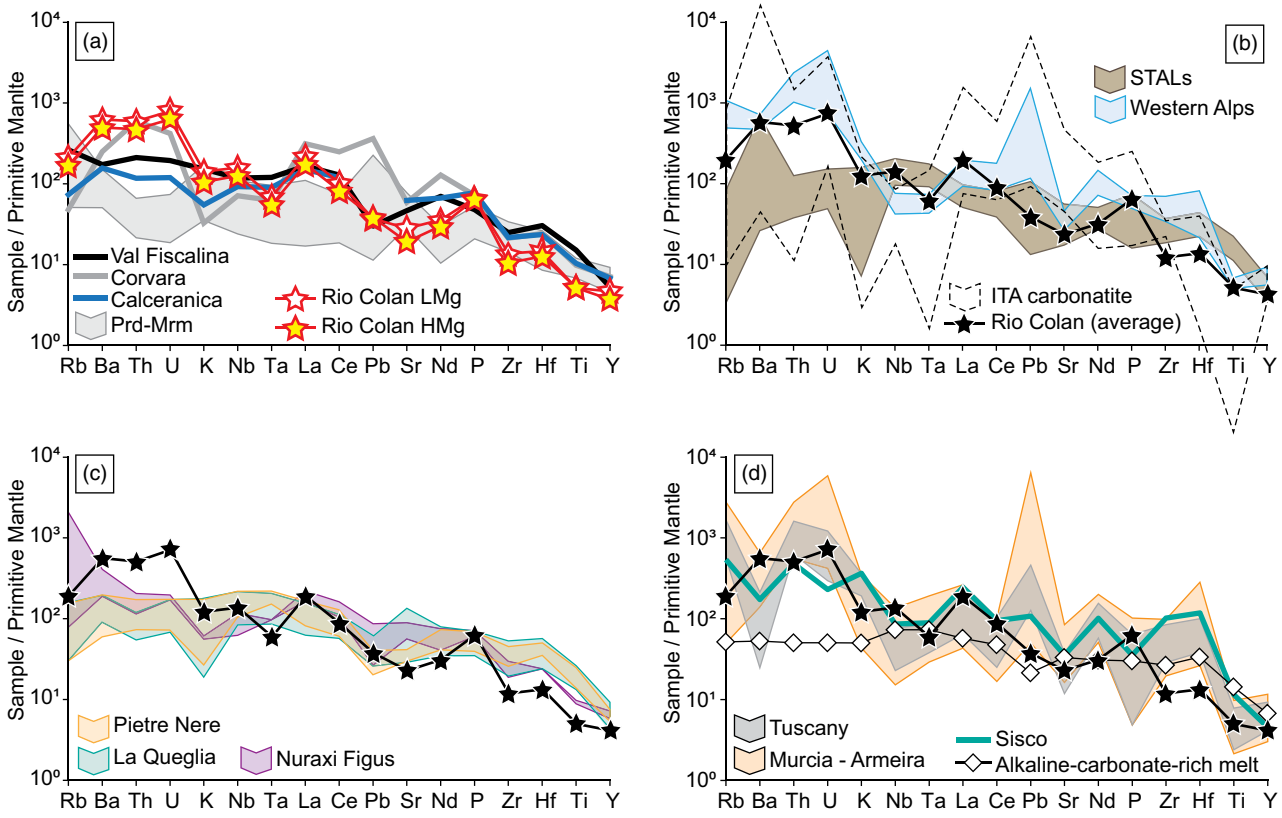


**Fig. 9.** (Colour online) Primitive-mantle normalized multi-element patterns for the Rio Colan olivine minettes and the other lamprophyres and lamproites of the Western Mediterranean. See Figures 7 and 8 for more details and data sources.

crustal components and underwent carbonatitic metasomatism. We stress that this carbonatitic metasomatism cannot be linked to the Quaternary Italian carbonatitic magmatism (Stoppa *et al.* 2016, 2019) due to different geochemical (Figs 8b, 9b; Section 5c) and, mostly, crystallization ages. Afterwards, distinct alkaline–carbonate-rich melts percolated through the metasomatized mantle source(s), leading to rutile-rich metasomatism. Since amphibole was not present in the sources of the Rio Colan magmas, a MARID-like source is excluded although some MARID xenoliths show Nb/Ta and Zr/Hf ratios similar to the Rio Colan olivine minettes (cf. fig. 6b in Aulbach *et al.* 2011). Accordingly, we argue that the source(s) was probably a rutile–phlogopite-bearing carbonated peridotite(s). These observations support those studies (Prelević *et al.* 2008, 2010; Stoppa *et al.* 2014; A Pandey *et al.* 2017*a*, *b*; Talukdar *et al.* 2018; R Pandey *et al.* 2019 and references therein) arguing for multiple metasomatic agents in the genesis of on–off craton lamprophyres and lamproites.

### 6.c. Geochronological and geodynamic implications

The Rio Colan dykes have a thickness not exceeding 60 cm, implying rapid cooling after intrusion. Since Brime *et al.* (2008) showed that the NE sector of the Italian Alps did not experience any thermal heating exceeding 300 °C, we can conclude that the apatite dates represent the age of intrusion and crystallization of the Rio Colan minettes. Our conclusion is supported by Pochon *et al.*'s (2016) modelling. Firstly, they showed that regardless of host-rock temperature, a mafic dyke with a thickness of less than 1 m solidifies instantaneously (<40 years; cf. fig. 7 in Pochon *et al.* 2016). Secondly, excluding post-emplacement high-temperature reheating, Pochon *et al.* (2016) demonstrated that the solidification time of a small-scale mafic/ultramafic intrusion and the time needed for an apatite to reach its closure temperature in a mafic system are almost identical. For instance, in a 60 m wide mafic body intruding a country rock at $T = 300$ °C and at a general cooling rate of 7 °C yr$^{-1}$, an apatite with a radius up to 50 μm has a closure temperature between 770 and 870 °C, which is reached in <20 years (Pochon *et al.* 2016). Given that Rio Colan dykes have a width $10^3$ times smaller than the dykes used by Pochon *et al.* (2016) and that our apatites have a radius ≤50 μm, it is very likely that apatites reached their closure temperature and crystallized almost instantaneously.

The unforced lower intercept ages of 23 ± 12 and 42 ± 21 Ma are similar within the error to those of the Oligocene (~34 to 30 Ma) Val Fiscalina and Western Alps lamprophyres (Lucchini *et al.* 1983; Owen 2008, and references therein), and consistent with the age of ~26 Ma that Carulli *et al.* (1987) previously suggested for the Rio Colan dykes, although no information was given about the methodology used to obtain that age. According to these ages, Rio Colan magmas would be linked to the Alpine–Apennine orogeny. Yet the unforced lower intercept ages show up to ~45 Ma difference compared to the forced discordia ages. Such a significant age variation may be due to the fact that apatites did not develop enough spread in common Pb / radiogenic Pb and therefore may strongly depend on the initial $^{207}Pb/^{206}Pb$ correction based on the Stacey and Kramers (1975) evolution model. Nonetheless, these anchored ages are fairly similar to the $^{206}Pb/^{238}U$ weighted mean ages that appear insensitive to the correction used (i.e. Thomson *et al.* 2012). The forced concordia and weighted mean ages together suggest that Rio Colan olivine minettes intruded and crystallized at

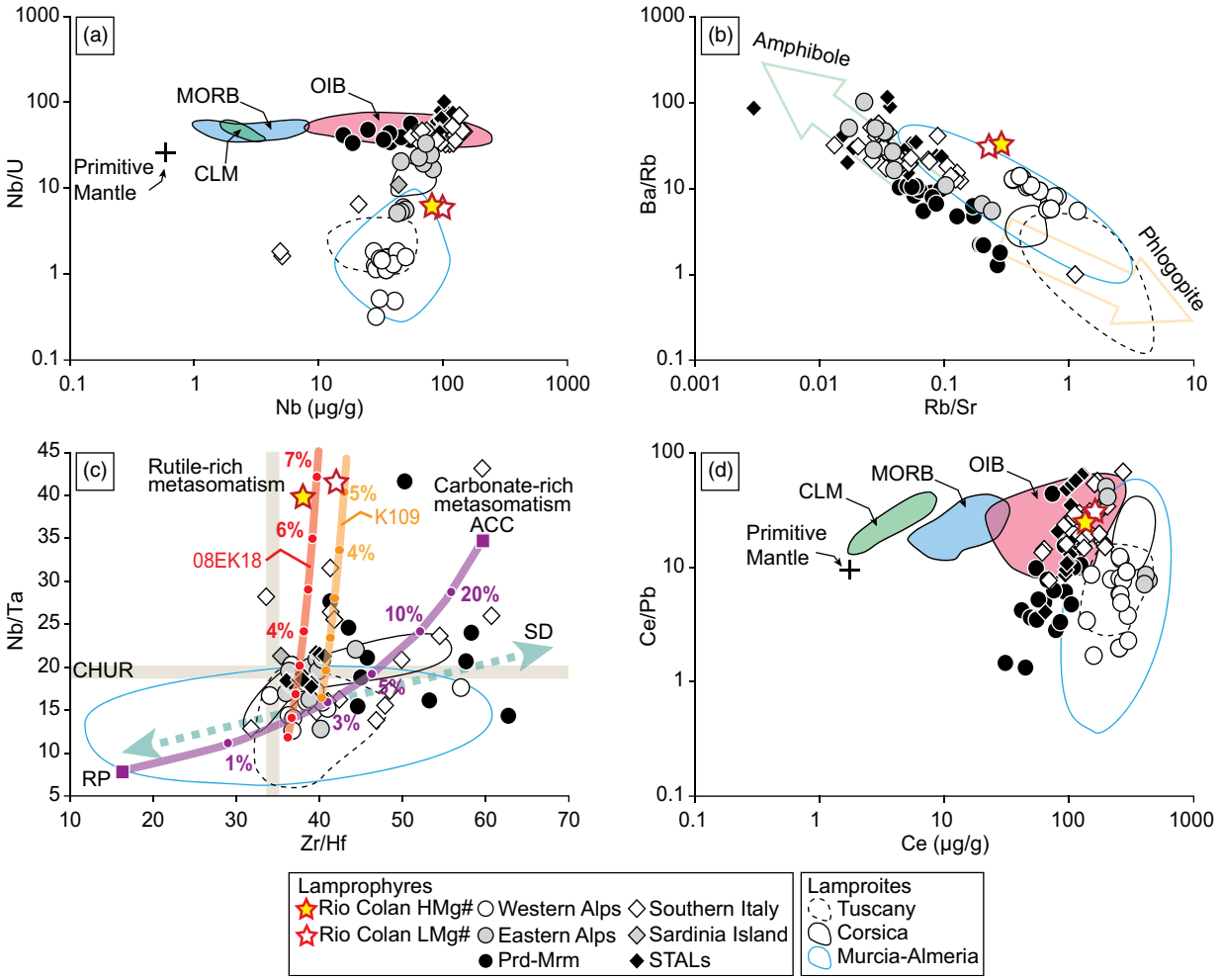


**Fig. 10.** (Colour online) Elemental ratios (µg/g). (a) Nb/U vs Nb, (b) Ba/Rb vs Rb/Sr, (c) Nb/Ta vs Zr/H and (d) Ce/Pb vs Ce. (a) and (d) are modified from Owen (2008); in (a) MORB is mid-ocean ridge basalt, OIB is ocean island basalt and CLM is continental lithosphere mantle. (b) is modified from Tommasini *et al*. 2011) and (c) from Aulbach *et al.* (2011). In (c), carbonate-rich and rutile-rich metasomatism trends are from Aulbach *et al.* (2011) and Guo *et al.* (2004), respectively; RP, ACC and SD represent the residual peridotite, the average composition of the carbonatite component and the silicate differentiation trend, respectively (after Aulbach *et al.* 2011). Data sources as in Figure 7.

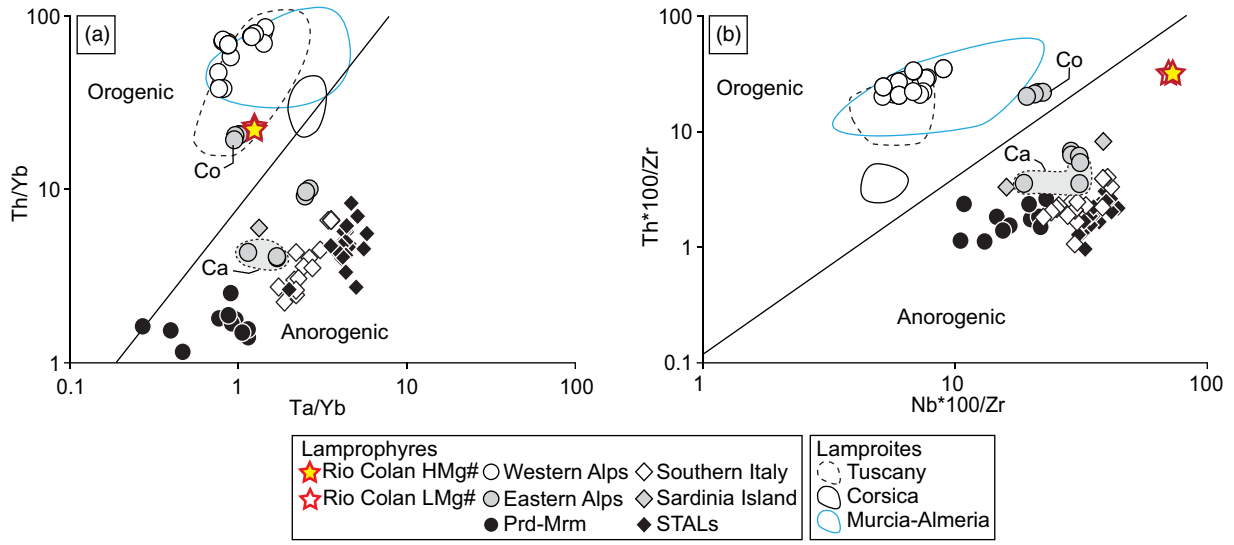


**Fig. 11.** (Colour online) Tectonomagmatic diagrams. (a) Th/Yb vs Ta/Yb and (b) Th*100/Zr vs Nb*100/Zr. In both diagrams, Co and Ca indicate Corvara in Badia and Calceranica lamprophyres. Data sources as in Figure 7.

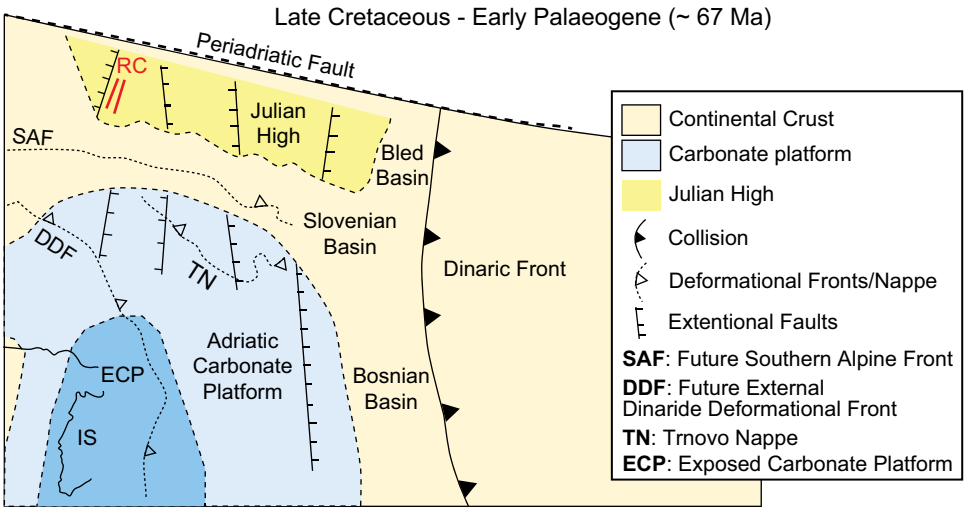


**Fig. 12.** (Colour online) Tectonic sketch map of the NE Alpine sector during the Late Cretaceous – Early Palaeogene limit (~67 Ma; modified after Goričan *et al.* 2018). The location of the Rio Colan olivine minettes (in red) in the Julian High, which represents the modern-day Julian Alps, is approximate.

67 ± 4 Ma (2SD; $n = 4$), as with the Corvara in Badia (68 ± 2 – 69 ± 3 Ma; Lucchini *et al.* 1983) and Calceranica (71 ± 2 Ma; Galassi *et al.* 1994) lamprophyres, indicating that Rio Colan olivine minettes intruded the Julian Alps during a period of regional extensional tectonics (Fig. 12; Goričan *et al.* 2018). The general NE–SW Rio Colan dykes orientation (Fig. 1c) is consistent with the Late Cretaceous coaxial stresses generated during the Eoalpine compressive stages when the European and African continental plates started to collide and the oceanic lithosphere to subduct (e.g. Csontos & Vörös, 2004). In this context, the Julian Alps were the Dinaric flexural foreland basin undergoing N–S and NW–SE extensional tectonics caused by the advance of the Dinaric front due to the eastward subduction of the Adria plate (Ponton, 2006, 2010; Goričan *et al.* 2018).

Further constraints are given by the Th/Yb vs Ta/Yb and Th*100/Zr vs Nb*100/Zr diagrams (Fig. 11a, b). These allow magmas generated from sources modified by subduction processes to be differentiated from those unrelated to such environments (e.g. Lustrino *et al.* 2016). During melting, Th is a mobile element and its enrichment over Yb and Ta indicates a subduction-related component. Similar is the case for Th when compared against Zr and Nb. Moreover, normalizing to Yb and Zr reduces the fractionation effect of clinopyroxene, mica, amphibole and feldspar (e.g. Owen, 2008). Rio Colan minettes show orogenic and anorogenic features (Fig. 11a, b), while the coeval Corvara in Badia and Calceranica lamprophyres plot in the orogenic and anorogenic fields, respectively. Because of this and the new ages here presented, we argue that the orogenic character shown in part by the Rio Colan magmas cannot be related to the Eoalpine orogeny but could reflect a local residual effect of an old orogenic event not completely exhausted. It must be noted that the volumes of the mantle source(s) involved in the Permo-Triassic magmatic event(s) in the Julian and Carnian Alps should have been orders of magnitude lower than in the neighbouring Dolomites, as evidenced by the strongly contrasting volumes of magmas emplaced between the two areas (e.g. De Min *et al.* 2020). In other words, the peridotitic source(s) of the Rio Colan olivine minettes display an old orogenic component because the mantle was less affected by the Permo-Triassic events underneath this extreme sector of the Italian Southern Alps. Moreover, these magmas crop out in an area that underwent extensional movements during the Late Cretaceous and witnessed the Pangaea break-up during the Triassic (De Min *et al.* 2020). As observed previously, it is interesting that high Nb/Ta ratios in many Lower Cretaceous to Miocene Italian lamprophyres can be explained by the percolation of alkaline–carbonate-rich melts through a carbonated peridotite. We argue that Middle Triassic alkaline–carbonate-rich melts triggered by the asthenospheric upwelling during the Pangaea break-up might have been the last agents that metasomatized the mantle before the Lower Cretaceous to Miocene Italian lamprophyric magmatism and would support the observations (i.e. Stoppa *et al.* 2014) that there is no relationship between metasomatism and recent Tethyan subduction.

## 7. Conclusions

New ultramafic dykes were found in the Julian Alps, in NE Italy. Petrographic and mineral chemical data indicate that Rio Colan dykes are olivine minettes. Rio Colan olivine minettes are one of the most primitive magmas among the Western Mediterranean lamprophyres and lamproites. The Rio Colan intrusions were generated from a strongly depleted peridotitic source that underwent different metasomatic processes before melting, leading it to evolve into a rutile–phlogopite-bearing carbonated peridotite. LA-MC-ICP-MS U–Pb geochronology applied to magmatic apatite suggests that these magmas intruded the Julian Alps at ~67 Ma during a period of extensional tectonics caused by the advance of the Dinaric front due to Alpine subduction towards the E. As this age is consistent with other Late Cretaceous lamprophyres cropping out in the Dolomitic sector, such extensional events might have affected larger parts of NE Italy. Given the above observations and the fact that Rio Colan olivine minettes intruded an area already affected by the tectonics related to the Triassic Pangaea break-up, the crustal and carbonatitic metasomatism may reflect some local residual effect of an old orogenic event not completely exhausted. In addition, the evidence that high Nb/Ta ratios in Rio Colan and other lamprophyres could be explained through middle-Triassic-related alkaline–carbonate-rich magmatism might imply that the last metasomatic event is not related to younger Tethyan subduction but rather to the Pangaea break-up.

**Supplementary material.** To view supplementary material for this article, please visit https://doi.org/10.1017/S0016756823000183

**Acknowledgements.** Backscattered images of the clinopyroxenes and cathodoluminescence of apatites analysed during this work were acquired by the Microscopy and Microanalysis Laboratory (LMic) of the Universidade Federal de Ouro Preto, a member of the Microscopy and Microanalysis Network of Minas Gerais State/Brazil/FAPEMIG. FN acknowledges Cristiane Gonçalves and Débora Vasconcelos de Oliveira (DEGEO/UFOP). FN thanks Cristiano Lana (DEGEO/AIRG/UFOP) for providing the U–Pb apatite ages and for taking part during the early stages of the manuscript. The manuscript benefited from discussions with Marco Venier (DMG/UNITS), Ana Černok (DMG/UNITS), Luca Ziberna (DMG/UNITS) and Samuel Bersan (UERJ). We thank Sarah Sherlock for the editorial handling. Three anonymous referees and reviews by Federico Casetta significantly improved the quality of the manuscript. No financial support was needed.

**Conflicts of interest.** The authors declare that they have no competing interests.

## References

**Aulbach S, O'Reilly SY and Pearson NJ** (2011) Constraints from eclogite and MARID xenoliths on origins of mantle Zr/Hf–Nb/Ta variability. *Contributions to Mineralogy and Petrology* **162**, 1047–62.

**Avanzinelli R, Sapienza GT and Conticelli S** (2012) The Cretaceous to Paleogene within-plate magmatism of Pachino-Capo Passero (southeastern Sicily) and Adria (La Queglia and Pietre Nere, southern Italy): geochemical and isotopic evidence against a plume-related origin of circum-Mediterranean magmas. *European Journal of Mineralogy* **24**, 73–96.

**Baier J, Audétat A and Keppler H** (2008) The origin of the negative niobium tantalum anomaly in subduction zone magmas. *Earth and Planetary Science Letters* **267**, 290–300.

**Becker M and Le Roex AP** (2006) Geochemistry of South African on- and off-craton, Group I and Group II kimberlites: petrogenesis and source region evolution. *Journal of Petrology* **47**, 673–703.

**Bianchini G, Beccaluva L and Siena F** (2008) Post-collisional and intraplate Cenozoic volcanism in the rifted Apennines/Adriatic domain. *Lithos* **101**, 125–40.

**Bigazzi G, Laurenzi MA, Principe C and Brocchini D** (1996) New geochronological data on igneous rocks and evaporites of the Pietre Nere point (Gargano Peninsula, Southern Italy). *Bollettino della Società Geologica Italiana* **115**, 439–48.

**Boynton WB** (1984) Cosmochemistry of rare earth elements: meteorite studies. In *Rare Earth Element Geochemistry* (ed P Henderson), pp. 63–114. Amsterdam: Elsevier.

**Bressan G, Barnaba C, Bragato P, Ponton M and Restivo A** (2018) Revised seismotectonic model of NE Italy and W Slovenia based on focal mechanism inversion. *Journal of Seismology* **22**, 1563–78.

**Bressan G, Bragato PL and Venturini C** (2003) Stress and strain tensors based on focal mechanisms in the seismotectonic framework of the Friuli-Venezia Giulia Region (Northeastern Italy). *Bulletin of the Seismological Society of America* **93**, 1280–97.

**Brime C, Perri MC, Pondrelli M, Spalletta C and Venturini C** (2008) Polyphase metamorphism in the eastern Carnic Alps (N Italy – S Austria): clay minerals and conodont Colour Alteration Index evidence. *International Journal of Earth Science* **97**, 1213–29.

**Canning JC, Henney P., Morrison MA and Gaskarth JW** (1996) Geochemistry of late Caledonian minettes from northern Britain: implications for the Caledonian sub-continental lithospheric mantle. *Mineralogical Magazine* **60**, 221–36.

**Carmichael I, Lange R and Luhr J** (1996) Quaternary minettes and associated volcanic rocks of Mascota, western Mexico: a consequence of plate extension above a subduction modified mantle wedge. *Contributions to Mineralogy and Petrology* **124**, 302–33.

**Carulli GB** (2006) *Carta Geologica del Friuli Venezia Giulia alla scala 1:50,000 – Note illustrative*. Florence: SELECA.

**Carulli GB, Cozzi A, Masetti A, Penarcic E, Podda F and Ponton M** (2003) Middle Triassic-Early Jurassic extensional tectonics in the Carnian Prealps (eastern Southern Alps, N.E. Italy). *Memorie di Scienze Geologiche* **54**, 151–4.

**Carulli GB, Frizzo P, Longo Salvdor G, Semenza E, Bianchin G, Mantovani F and Mezzacasa G** (1987) La geologia della zona tra il T. Chiarzò e il F. Fella (Alpi Carniche). 4 carte geologiche 1:20,000. *Giornale di Geologia* s.3a, **49/1**, 1–32.

**Casalini M, Avanzinelli R, Tommasini S, Natali C, Bianchini G, Prelevic D, Matteir M and Conticelli S** (2022) Petrogenesis of Mediterranean lamproites and associated rocks: the role of overprinted metasomatic events in the post-collisional lithospheric upper mantle. In *Lamprophyres, Lamproites and Related Rocks: Tracers to Supercontinent Cycles and Metallogenesis* (eds L Krmiček and NV Chalapathi Rao), pp. 271–96. *Geological Society of London, Special Publication* no. **513**.

**Casetta F, Ickert RB, Mark DF, Bonadiman C, Giacomoni PP, Ntaflos T and Coltorti M** (2019) The alkaline lamprophyres of the Dolomitic area (Southern Alps, Italy): markers of the Late Triassic change from orogenic-like to anorogenic magmatism. *Journal of Petrology* **60**, 1263–98.

**Casetta F, Ickert RB, Mark DF, Giacomoni PP, Bonadiman C, Ntaflos T, Zanetti A and Coltorti M** (2021) The Variscan subduction inheritance in the Southern Alps sub-continental lithospheric mantle: clues from the Middle Triassic shoshonitic magmatism of the Dolomites (NE Italy). *Lithos* **380–381**, 105856.

**Chalapathi Rao NV, Gibson SA, Pyle DM and Dickin AP** (2004) Petrogenesis of Proterozoic lamproites and kimberlites from the Cuddapah Basin and Dharwar Craton, Southern India. *Journal of Petrology* **45**, 907–48.

**Chauvel C, Hoffmann AW and Vidal P** (1992) HIMU-EM: the French-Polynesian connection. *Earth and Planetary Science Letters* **110**, 99–119.

**Chew DM, Sylvester PJ and Tubrett MN** (2011) U–Pb and Th–Pb dating of apatite by LA-ICPMS. *Chemical Geology* **280**, 200–16.

**Choi E, Fiorentini ML, Giuliani A, Foley F, Stephen MR and Taylor WR** (2020) Subduction-related petrogenesis of Late Archean calc-alkaline lamprophyres in the Yilgarn Craton (Western Australia). *Precambrian Research* **338**, 105550.

**Conticelli S, Guarnieri L, Farinelli A, Mattei M, Avanzinelli R, Bianchini G, Boari E, Tommasini S, Tiepolo M, Prelević D and Venturelli G** (2009) Trace elements and Sr-Nd-Pb isotopes of K-rich, shoshonitic, and calc-alkaline magmatism of the Western Mediterranean region: genesis of ultrapotassic to calc-alkaline magmatic associations in a post-collisional geodynamic setting. *Lithos* **107**, 68–92.

**Cundari A and Comin-Chiaramonti P** (1996) Mineral chemistry of alkaline rocks from the Asunción -Sapucai Graben (Central-Eastern Paraguay). In *Alkaline Magmatism in Central-Eastern Paraguay: Relationships with Coeval Magmatism in Brazil* (eds P Comin-Chiaramonti and CB Gomes), pp. 181–94. São Paulo: Edusp/Fapesp.

**Cundari A and Ferguson AK** (1982) Significance of the pyroxene chemistry from leucite-bearing and related assemblages. *Mineralogische und Petrographische Mitteilungen* **30**, 189–204.

**Dalton HB, Giuliani A, O'Brien H, Phillips D and Hergt J** (2019) Petrogenesis of a hybrid cluster of evolved kimberlites and ultramafic lamprophyres in the Kuusamo area, Finland. *Journal of Petrology* **60**, 2025–50.

**De Min A, Velicogna D, Ziberna L, Marzoli A, Chiaradia M and Alberti A** (2020) Triassic magmatism in the European Southern Alps as an early phase of Pangea break-up. *Geological Magazine* **157**, 1800–22.

**Esperança S and Holloway JR** (1987) On the origin of some mica-lamprophyres: experimental evidence from a mafic minette. *Contributions to Mineralogy and Petrology* **95**, 207–16.

**Fitzpayne A, Giuliani A, Hergt J, Phillips D and Janney P** (2018) New geochemical constraints on the origins of MARID and PIC rocks: implications for mantle metasomatism and mantle-derived potassic magmatism. *Lithos* **318–319**, 478–93.

**Fitzpayne A, Giuliani A, Roland M, Hergt Janney P and Phillips D** (2019) Progressive metasomatism of the mantle by kimberlite melts: Sr–Nd–Hf–Pb isotope compositions of MARID and PIC minerals. *Earth and Planetary Science Letters* **509**, 15–26.

**Foley S** (1992) Vein-plus-wall-rock melting mechanisms in the lithosphere and the origin of potassic alkaline magmas. *Lithos* **28**, 435–53.

**Foley S, Barth MG and Jenner GA** (2000) Rutile/melt partition coefficients for trace elements and an assessment of the influence of rutile on the trace element characteristics of subduction zone magmas. *Geochimica et Cosmochimica Acta* **64**, 933–8.

**Foley S, Tiepolo M and Vannucci R** (2002) Growth of early continental crust controlled by melting of amphibolite in subduction zones. *Nature* **417**, 837–40.

**Foley S, Venturelli G, Green DH and Toscani L** (1987) The ultrapotassic rocks: characteristics, classification, and constraints for petrological models. *Earth-Science Reviews* **24**, 81–134.

**Galassi B, Monose A, Ogniben G, Siena F and Vaccaro C** (1994) Age and nature of lamprophyric dyke at Calceranic (Trento). *Mineralogica et Petrographica Acta* **37**, 163–71.

**Giuliani A, Phillips D, Woodhead JD, Kamenetsky VS, Fiorentini ML, Maas R, Soltys A and Armstrong RA** (2015). Did diamond-bearing orangeites originate from MARID veined peridotites in the lithospheric mantle? *Nature Communications* 6, 6387. https://doi.org/10.1038/ncomms7837.

**Goričan S, Žibret L, Košir A, Kukoč D and Horvat A** (2018) Stratigraphic correlation and structural position of Lower Cretaceous flysch-type deposits in the eastern Southern Alps (NW Slovenia). *International Journal of Earth Science* **107**, 2933–53.

**Grégoire M, Bell D and le Roex A** (2002) Trace element geochemistry of phlogopite-rich mafic mantle xenoliths: their classification and their relationship to phlogopite-bearing peridotites and kimberlites revisited. *Contributions to Mineralogy and Petrology* **142**, 603–25.

**Guo F, Fan W, Wang Y and Zhang M** (2004) Origin of early Cretaceous calc-alkaline lamprophyres from the Sulu orogen in eastern China: implications for enrichment processes beneath continental collisional belt. *Lithos* **78**, 291–305.

**Ketcham RA** (2015) Technical Note: Calculation of stoichiometry from EMP data for apatite and other phases with mixing on monovalent anion sites. *American Mineralogist* **100**, 1620–3.

**Krmíček L and Chalapathi Rao NV** (2022) Lamprophyres, lamproites and related rocks as tracers to supercontinent cycles and metallogenesis. In *Lamprophyres, Lamproites and Related Rocks: Tracers to Supercontinent Cycles and Metallogenesis* (eds L Krmiček and NV Chalapathi Rao), pp. 1–16. *Geological Society of London, Special Publication* no. **513**.

**Lana C, Farina F, Gerdes A, Alkmim A, Gonçalves GO and Jardim AC** (2017) Characterization of zircon reference materials via high precision U–Pb LA-MC-ICP-MS. *Journal of Analytical Atomic Spectrometry* **32**, 2011–23.

**Lana C, Gonçalves GO, Mazoz A, Buick I, Kamo S, Scholz S, Wang H, Moreira H, Babinski M and Queiroga G** (2021) Assessing the U-Pb, Sm-Nd and Sr-Sr isotopic compositions of the Sumé Apatite as a reference material for LA-ICP-MS analysis. *Geostandards and Geoanalytical Research* **46**, 71–95.

**Le Maitre RW, Streckeisen A, Zanettin B, Le Bas MJ, Bonin B and Bateman P** (2002) *Igneous Rocks. A Classification and Glossary of Terms. Recommendations of the IUGS Subcomission on the Systematics of Igneous Rocks*. Cambridge: Cambridge University Press.

**Lucchini F, Simboli G, Zenatti A, Barbieri M, Nicoletti M and Petrucciani C** (1983) Petrochimica e dati radiometrici K/Ar e Rb/Sr dei "filoni basici" di Corvara in Badia e de lamprofiri di Val Fiscalina (Dolomiti orientali). Revisione classificativa ed implicazioni genetiche nel quadro del magmatismo filoniano delle Alpi. *Mineralogica et Petrographica Acta* **27**, 233–49.

**Lustrino M, Agostini S, Chalal Y, Fedele L, Stagno V, Colombi F and Bouguerra A** (2016) Exotic lamproites or normal ultrapotassic rocks? The Late Miocene volcanic rocks from Kef Hahouner, NE Algeria, in the frame of the circum-Mediterranean lamproites. *Journal of Volcanology and Geothermal Research* **327**, 539–53.

**Maccioni L and Marchi M** (1994) Eocene magmatic activity in Sardinia – Italy (new occurrence of alkaline lamprophyre). *Mineralogica et Petrographica Acta* **39**, 199–210.

**Mazzeo FC, Arienzo I, Aulinas M, Casalini M, Di Renzo V and D'Antonio M** (2018) Mineralogical, geochemical and isotopic characteristics of alkaline mafic igneous rocks from Punta delle Pietre Nere (Gargano, Southern Italy). *Lithos* **308–309**, 316–28.

**McDonough WF and Sun SS** (1995) The composition of the Earth. *Chemical Geology* **120**, 223–53.

**Miller C, Thöni M, Goessler W and Tessadri R** (2011) Origin and age of the Eisenkappel gabbro to granite suite (Carinthia, SE Austrian Alps). *Lithos* **125**, 434–48.

**Mitchell RH** (1995). *Kimberlites, orangeites and Related Rocks*. New York: Plenum Press, 410 pp.

**Mitchell RH and Bergman SC** (1991) *Petrology of Lamproites*. New York: Plenum Press, 447 pp.

**Moayyed M, Moazzena M, Calagaria AA, Jahangiria A and Modjarrad M** (2008) Geochemistry and petrogenesis of lamprophyric dykes and the associated rocks from Eslamy peninsula, NW Iran: implications for deep-mantle metasomatism. *Chemie der Erde Geochemistry* **68**, 141–54.

**O'Brien HE, Irving AJ and McCallum IS** (1991) Eocene potassic magmatism in the Highwood Mountains, Montana: petrology, geochemistry and tectonic implications. *Journal of Geophysical Research* **96B**, 13237–60.

**Ohta T and Arai H** (2007) Statistical empirical index of chemical weathering in igneous rocks: a new tool for evaluating the degree of weathering. *Chemical Geology* **240**, 280–97.

**Owen JP** (2008) Geochemistry of lamprophyres from the Western Alps, Italy: implications for the origin of an enriched isotopic component in the Italian mantle. *Contributions to Mineralogy and Petrology* **155**, 341–62.

**Pandey A, Chalapathi Rao NV, Chakrabarti R, Pandit D, Pankaj P, Kumar A and Sahoo S** (2017a) Petrogenesis of a Mesoproterozoic shoshonitic lamprophyre dyke from the Wajrakarur kimberlite field, eastern Dharwar craton, southern India: geochemical and Sr-Nd isotopic evidence for a modified subcontinental lithospheric mantle source. *Lithos* **292–293**, 218–33.

**Pandey A, Chalapathi Rao NV, Chakrabarti R, Pankaj P, Pandit D, Pandey R and Sahoo S** (2018) Post-collisional calc-alkaline lamprophyre from Kadiri greenstone belt: evidence for the Neoarchean convergence related evolution of Eastern Dharwar Craton and its schist belts. *Lithos* **320–321**, 105–17.

**Pandey A, Chalapathi Rao NV, Pandit D, Pankaj P, Pandey R, Sahoo S and Kumar A** (2017b) Subduction-tectonics in the evolution of the eastern Dharwar craton, southern India: insights from the post-collisional calc-alkaline lamprophyres at the western margin of the Cuddapah basin. *Precambrian Research* **298**, 235–51.

**Pandey R, Pandey A, Chalapathi Rao NV, Belyatsky B, Choudhary AK, Lehmann B, Pandit D and Dhote P** (2019) Petrogenesis of end-Cretaceous/Early Eocene lamprophyres from the Deccan Large Igneous Province: constraints on plume-lithosphere interaction and the post-Deccan lithosphere-asthenosphere boundary (LAB) beneath NW India. *Lithos* **346–347**, 105–39.

**Patiño Douce AE, Roden M, Chaumba J, Fleisher C and Yogodzinski G** (2011) Compositional variability of terrestrial mantle apatites, thermodynamic modeling ofapatite volatile contents, and the halogen and water budgets of planetary mantles. *Chemical Geology* **288**, 14–31.

**Peccerillo A and Martinotti G** (2006) The Western Mediterranean lamproitic magmatism: origin and geodynamic significance. *Terra Nova* **18**, 109–17.

**Pfänder JA, Munker C, Stracke A and Mezger K** (2007) Nb/Ta and Zr/Hf in ocean island basalts: implications for crust–mantle differentiation and the fate of Niobium. *Earth and Planetary Science Letters* **254**, 158–72.

**Pilet S, Baker MB and Stolper EM** (2008) Metasomatized lithosphere and the origin of alkaline lavas. *Science* **320**, 916–919.

**Pochon A, Poujol M, Gloaguen E, Branquet Y, Cagnard F, Gumiaux C and Gapais D** (2016) U-Pb LA-ICP-MS dating of apatite in mafic rocks: evidence for a major magmatic event at the Devonian-Carboniferous boundary in the Armorican Massif (France). *American Mineralogist* **101**, 2430–42.

**Ponton M** (2006) Tettonica estensionale del Senoniano nel Gruppo del Montasio (Alpi Meridionali orientali). *Gortania, Atti del Museo Friulano di Storia Nazionale* **27**, 7–16.

**Ponton M** (2010) *Architettura delle Alpi Friulane*. Pubblicazione no. 52. Udine: Museo Friulano di Storia Naturale, 79 pp.

**Prelević D, Foley SF, Romer RL and Conticelli S** (2008) Mediterranean Tertiary lamproites: multicomponent melts in post-collisional geodynamics. *Geochimica et Cosmochimica Acta* **72**, 2125–56.

**Prelević D, Stracke A, Foley SF, Romer RL and Conticelli S** (2010) Hf isotope compositions of Mediterranean lamproites: mixing of melts from asthenosphere and crustally contaminated mantle lithosphere. *Lithos* **119**, 297–312.

**Righter K. and Carmichael ISE** (1996) Phase equilibria of phlogopite lamprophyres from western Mexico; biotite-liquid equilibria and P–T estimates for biotite-bearing igneous rocks. *Contributions to Mineralogy and Petrology* **123**, 1–21.

**Rukhlov AS, Blinova AI and Pawlowicz JG** (2013) Geochemistry, mineralogy and petrology of the Eocene potassic magmatism from the Milk River area, southern Africa, and Sweet Grass Hills, northern Montana. *Chemical Geology* **353**, 280–302.

**Soltys A, Giuliani A and Phillips D** (2020) Apatite compositions and groundmass mineralogy record divergent melt/fluid evolution trajectories in coherent kimberlites caused by differing emplacement mechanisms. *Contribution to Mineralogy and Petrology* **175**, 1–20.

**Stacey JS and Kramers JD** (1975) Approximation of terrestrial lead isotope evolution by a two-stage model. *Earth and Planetary Science Letters* **26**, 207–21.

**Stoppa F** (2008) Alkaline and ultramafic lamprophyres in Italy: distribution, mineral phases and bulk rock data. In *Deep Seated Magmatism: Its Sources and Plumes* (ed. NV Vladykin), pp. 209–38. Irkutsk: Glazkovskaya Printing House.

**Stoppa F, Pirajno F, Schiazza M and Vladykin NV** (2016) State of the art: Italian carbonatites and their potential for critical-metal deposits. *Gondwana Research* **37**,152–71.

**Stoppa F, Rukhlov AS, Bell K, Schiazza M and Vichi G** (2014) Lamprophyres of Italy: early Cretaceous alkaline lamprophyres of Southern Tuscany, Italy. *Lithos* **188**, 97–112.

**Stoppa F, Schiazza M, Rosatelli G and Castorina F** (2019) Italian carbonatite system: from mantle to ore-deposit. *Ore Geology Reviews* **114**, 103041.

**Sun SS and McDonough QF** (1989) Chemical and isotopic systematics of oceanic basalts; implications for mantle compositions and processes. In *Magmatism in the Ocean Basins* (eds AD Saunders and MJ Norry), pp. 313–45. Geological Society of London, Special Publication no. 42.

**Talukdar D, Pandey A, Chalapathi Rao NV, Kumar A, Pandit D, Belyatsky B and Lehmann B** (2018) Petrology and geochemistry of the Mesoproterozoic Vattikod lamproites, Eastern Dharwar Craton, southern India: evidence for multiple enrichment of sub-continental lithospheric mantle and links with amalgamation and break-up of the Columbia supercontinent. *Contributions to Mineralogy and Petrology* **173**, 67.

**Tappe S, Foley SF, Jenner GA, Heaman LM, Kjarsgaard BA, Romer RL, Stracke A, Joyce N and Hoefs J** (2006) Genesis of ultramafic lamprophyres and carbonatites at Aillik Bay, Labrador: a consequence of incipient lithospheric thinning beneath the North Atlantic Craton. *Journal of Petrology* **47**, 1261–315.

**Tappe S, Foley SF, Kjarsgaard BA, Romer, RL, Heaman LM, Stracke A and Jenner GA** (2008) Between carbonatite and lamproite: diamondiferous Torngat ultramafic lamprophyres formed by carbonate-fluxed melting of cratonic MARID-type metasomes. *Geochimica et Cosmochimica Acta* **72**, 3258–86.

**Tappe S, Jenner GA, Foley SF, Heaman L, Besserer D, Kjarsgaard BA and Ryan B** (2004) Torngat ultramafic lamprophyres and their relation to the North Atlantic Alkaline Province. *Lithos* **76**, 491–518.

**Thomson SN, Gehrels GE, Ruiz J and Buchwaldt R** (2012) Routine low-damage apatite U–Pb dating using laser ablation-multicollector-ICPMS. *Geochemistry, Geophysics Geosystems* **13**, Q0AA21. doi: 10.1029/2011GC003928.

**Tiepolo M, Vannucci R, Oberti R, Foley S, Bottazzi P and Zanetti A** (2000) Nb and Ta incorporation and fractionation in titanian pargasite and kaersutite: crystal-chemical constraints and implications for natural systems, *Earth and Planetary Science Letters* **176**, 185–201.

**Tingey DG, Christiansen EH, Best MG, Ruiz J and Lux DR** (1991) Tertiary minette and melanephelinite dikes, Wasatch Plateau, Utah: records of mantle heterogeneities and changing tectonics. *Journal of Geophysical Research* **96**, 13529–44.

**Tommasini S, Avanzinelli R and Conticelli S** (2011) The Th/La and Sm/La conundrum of the Tethyan realm lamproite. *Earth and Planetary Science Letters* **301**, 469–78.

**Vichi G, Perna MG, Ambrosio F, Rosatelli G, Cirillo D, Broom-Fendley S, Vladykin NV, Zacccaria D and Stoppa F** (2022) La Queglia carbonatitic melnöite: a notable example of an ultra-alkaline rock variant in Italy. *Mineralogy and Petrology* https://doi.org/10.1007/s00710-022-00792-0.

**Vichi G, Stoppa F and Wall F** (2005) The carbonate fraction in carbonatitic Italian lamprophyres. *Lithos* **85**, 154–70.

**Zanferrari A, Masetti D, Monegato G and Poli Me** (2013) Geological map and explanatory notes of the Geological Map of Italy at the scale 1:50.000: Sheet 049 "Gemona del Friuli" ISPRA - Servizio Geologico d'Italia - Regione Autonoma Friuli Venezia Giulia (2013), p. 262